An Experimental Study of Segmented Two-Phase Flow and Heat Transfer Characteristics in a Microchannel

Ms. Pansunee Suwankamnerd B.Eng. (Mechanical Engineering)

A Thesis Submitted in Partial Fulfillment
of the Requirements for
the Degree of Master of Engineering (Mechanical Engineering)
Faculty of Engineering
King Mongkut's University of Technology Thonburi
2013

Thesis Committee

……..... (Prof. Somchart Chantasiriwan, Ph.D.)	Chairman of Thesis Committee
……..... (Prof. Somchai Wongwises, Ph.D., Dr.-Ing.)	Member and Thesis advisor
……..... (Asst. Prof. Surachai Sanitjai, Ph.D.)	Member
……..... (Asst. Prof. Wishsanuruk Wechsatol, Ph.D.)	Member

Thesis Title	An Experimental Study of Segmented Two-Phase Flow and Heat Transfer Characteristics in a Microchannel
Thesis Credits	12
Candidate	Ms. Pansunee Suwankamnerd
Thesis Advisor	Prof. Dr. Somchai Wongwises
Program	Master of Engineering
Field of Study	Mechanical Engineering
Department	Mechanical Engineering
Faculty	Engineering
B.E.	2013

Abstract

Cooling systems are needed for the electronic devices in order to operate efficiently. Because the size of the equipment is decreased to the micro scale, research on the heat transfer characteristics in a microchannel heat sink is needed. In this work, the nonboiling of segmented air-water flow was proposed to be an alternative method for heat transfer enhancement in a microchannel heat sink compared to using single-phase water cooling. The experiment was conducted with two-phase air-water flow in a single rectangular microchannel with a hydraulic diameter of 267 μm. The test section was made of copper. For a clear understanding, a two-phase flow pattern, a pressure drop, and heat transfer characteristics in the low Reynolds number of air-water flow were identified. The results show that segmented, throat-annular, throat-annular/liquid, and annular flow were observed in the test section. A flow pattern map was created and compared with the previous maps. The pressure drop can be predicted by the homogeneous flow model and the Friedel correlation separated flow model. In the heat transfer characteristics, the results demonstrated that the Nusselt number of segmented flow increases up to 1.2 times over the single-phase flow.

Keywords: Microchannel/Segmented flow/Flow pattern/Nusselt number/Pressure drop

หัวข้อวิทยานิพนธ์	การศึกษาเชิงทดลองของลักษณะการไหลสองเฟสแบบเซกเมนต์และการถ่ายเทความร้อนในอุปกรณ์ระบายความร้อนที่มีช่องทางการไหลขนาดเล็กมาก
หน่วยกิต	12
ผู้เขียน	นางสาวปานสุนี สุวรรณกำเนิด
อาจารย์ที่ปรึกษา	ศ. ดร.สมชาย วงศ์วิเศษ
หลักสูตร	วิศวกรรมศาสตรมหาบัณฑิต
สาขาวิชา	วิศวกรรมเครื่องกล
ภาควิชา	วิศวกรรมเครื่องกล
คณะ	วิศวกรรมศาสตร์
พ.ศ.	2556

บทคัดย่อ

การถ่ายเทความร้อนให้แก่อุปกรณ์อิเล็กทรอนิกส์เป็นสิ่งจำเป็นเพื่อให้อุปกรณ์สามารถทำงานได้เต็มประสิทธิภาพ แต่ปัจจุบันอุปกรณ์อิเล็กทรอนิกส์มีขนาดลดลงอย่างต่อเนื่อง งานวิจัยจึงควรให้ความสำคัญต่อการศึกษาและทำความเข้าใจเกี่ยวกับการถ่ายเทความร้อนให้แก่อุปกรณ์ขนาดเล็กเพื่อให้ได้มาซึ่งวิธีที่เหมาะสม งานวิจัยนี้ได้ทำการทดลองเกี่ยวกับการไหลสองเฟสในช่องทางการไหลขนาดเล็กมากโดยหน้าตัดของช่องทางการไหลเป็นสี่เหลี่ยมที่ทำจากทองแดง มีเส้นผ่าศูนย์กลางไฮดรอลิกส์ขนาด 267 ไมโครเมตร รูปแบบการไหล ความดันลด และการถ่ายเทความร้อนจะเกิดในช่วงที่มีค่าเรย์โนลด์ต่ำที่ใช้น้ำและอากาศเป็นสารทำงานให้แก่ระบบ จากผลการทดลองพบว่า รูปแบบการไหลที่เกิดขึ้นคือ segmented, throat-annular, throat-annular/liquid และ annular มีแผนที่รูปแบบการไหลที่มีลักษณะเฉพาะตัว และสามารถทำนายความดันลดได้ทั้งการใช้โมเดลความดันลดแบบ รูปแบบการไหลแบบเนื้อเดียว และรูปแบบการไหลแบบแยกส่วน และสำหรับลักษณะการถ่ายเทความร้อนจากการทดลองพบว่า การไหลสองเฟสแบบเซกเมนต์สามารถเพิ่มความสามารถในการถ่ายเทความร้อนให้กับช่องทางการไหลได้เพิ่มขึ้นสูงถึง 1.2 เท่าเมื่อเปรียบเทียบกับการไหลเฟสเดียวของน้ำ

คำสำคัญ : ช่องทางการไหลขนาดเล็กมาก/การไหลแบบเซกเมนต์/รูปแบบการไหล/ค่านัสเซลต์/ความดันลด

ACKNOWLEDGEMENT

This research work would not have been possible without the help and active collaboration of many people to whom I acknowledge my indebtedness and sincere gratitude and appreciation. Firstly, I would like to express sincere thanks to my advisor, Prof. Dr. Somchai Wongwises, for his valuable suggestion, attentive interest, and kind recommendations in the present study. Sincere thank to the members of my dissertation committee for their valuable time and suggestions. I am very grateful to the National Research Council of Thailand (NRCT) for providing the scholarship and financial support for this thesis in 2012. Thank you the student in the FUTURE Lab (Fluid Mechanics, Thermal Engineering and Multiphase Flow Research Laboratory) at mechanical engineering, King Mongkut's University of Technology Thonburi, for their help and guidance during my study. Finally, I would like to thank my family for their support, encouragement, endless love and understanding throughout my study program.

CONTENTS

LIST OF TABLES

LIST OF FIGURES

LIST OF SYMBOLS

A_{ch}	surface area of the test section, m^2
AR	aspect ratio of channel
C	coefficient C value
C_c	coefficient of contraction
C_p	specific heat (J/kgK)
D_h	hydraulic diameter of channel, m
Fr_H	the dimensionless factor
f	friction factor
G	mass flux, kg/m^2s
g	gravitational acceleration, m/s^2
H	channel height, m
h	heat trabsfer coefficient (W/m^2K)
k	thermal conductivity (W/mK)
L	channel length, m
Nu	Nusselt number
P	pressure, Pa
Q_{bulk}	heat transfer, W
q''	heat flux, W/m^2
Re	Reynolds number
T	Temperature ,°C, K
U	superficial velocity, m/s

V	volume flow rate, m^3/s
W	channel width, m
We	Weber number
X_{vv}	Martinelli parameter for larminar-larminar flow
x	quality

Greek symbols

β	gas volumetric ratio
ρ	density, kg/m^3
α	void fraction
μ	dynamic viscosity, kg/m s
ρ	density, kg/m^3
γ	ratio of the cross-sectional flow area in the flow passage connected to the channel test section to that in the channel test section
ϕ	two-phase frictional multiplier
ΔP	pressure drop, kPa/m

Subscripts

ch	channel
c/e	contraction/expansion
exp	experimental value
f	fluid
G	gas
GS	gas superficial velocity
H	homogeneous flow
L	liquid
LS	liquid superficial velocity

pred	predicted value
s	surface
TP	two-phase

APPENDICES

APPENDIX A. THE EXAMPLES OF UNCERTAINTY CALCULATIONS

1. The uncertainty of the superficial velocity of gas (δU_{GS})

$$\delta U_{GS} = \sqrt{\left(\frac{\partial U_{GS}}{\partial \dot{m}_G}\delta \dot{m}_G\right)^2 + \left(\frac{\partial U_{GS}}{\partial A}\delta A\right)^2}$$

$$U_{GS} = \frac{\dot{m}_G}{\rho_G A} = \frac{(9.667\times10^{-8})\frac{kg}{s}}{(1.1302)\frac{kg}{m^3}\times(8\times10^{-8})m^2} = 1.0692 m/s$$

$$\dot{m}_G = \rho_G V_G = (1.1302)\frac{kg}{m^3}(8.333\times10^{-8})\frac{m^3}{s} = 9.418\times10^{-8}\frac{kg}{s}$$

$$A = WL$$

$$\frac{\partial A}{\partial L} = W$$

$$\frac{\partial A}{\partial W} = L$$

$$\delta A = \sqrt{\left(\frac{\partial A}{\partial W}.\delta W\right)^2 + \left(\frac{\partial A}{\partial L}.\delta L\right)^2}$$

$$\delta A = \sqrt{\left((0.0002mm)(10^{-5}mm)\right)^2 + \left((0.0004mm)(2\times10^{-5}mm)\right)^2}$$

$$\delta A = \pm 8.246\times10^{-9} m^2$$

$$\frac{\delta A}{A}\times100 = \frac{\pm8.246\times10^{-9}}{8\times10^{-8}}\times100 = 10.3\%$$

$$\delta \dot{m}_G = \left(9.667\times10^{-8}\right)\frac{kg}{s}(0.08) = 7.733\times10^{-9}\frac{kg}{s}$$

$$\frac{\partial U_{GS}}{\partial \dot{m}_G} = \frac{1}{\rho_G A} = \frac{1}{1.1302\frac{kg}{m^3}\left(0.0002\times0.0004m^2\right)} = 11059989\frac{m}{kg}$$

$$\frac{\partial U_{GS}}{\partial A} = \frac{\dot{m}_G}{\rho_G A^2} = \frac{9.667\times10^{-8}\frac{kg}{s}}{1.1302\frac{kg}{m^3}\left(0.0002\times0.0004\right)^2 m^4} = 13364614 s^{-1}m^{-1}$$

so

$$\delta U_{GS} = \sqrt{\left(11059989\frac{m}{kg}\left(7.733\times10^{-9}\right)\frac{kg}{s}\right)^2 + \left(\left(13364614\right)s^{-1}m^{-1}\left(8.246\times10^{-9}\right)m^2\right)^2}$$

$$\delta U_{GS} = \pm 0.1368 m/s$$

$$\frac{\delta U_{GS}}{U_{GS}} \times 100 = \frac{\pm 0.1368}{1.06913} \times 100 = 12.8\%$$

2. The uncertainty of the superficial velocity of liquid (δU_{LS})

$$\delta U_{LS} = \sqrt{\left(\frac{\partial U_{LS}}{\partial \dot{m}_L} \delta \dot{m}_L \right)^2 + \left(\frac{\partial U_{LS}}{\partial A} \delta A \right)^2}$$

$$U_{LS} = \frac{\dot{m}_L}{\rho_L A} = \frac{(2.082 \times 10^{-6}) \frac{kg}{s}}{(992.08) \frac{kg}{m^3} \times (8 \times 10^{-8}) m^2} = 0.0262 m/s$$

$$\dot{m}_L = \rho_L V_L = (992.08) \frac{kg}{m^3} (2.082 \times 10^{-9}) \frac{m^3}{s} = 2.066 \times 10^{-6} \frac{kg}{s}$$

$$\delta \dot{m}_L = 2.082 \times 10^{-6} \frac{kg}{s} (0.001) = 2.082 \times 10^{-9} \frac{kg}{s}$$

$$\delta A = \pm 8.246 \times 10^{-9} m^2$$

$$\frac{\partial U_{LS}}{\partial \dot{m}_L} = \frac{1}{\rho_L A} = \frac{1}{992.08 \frac{kg}{m^3} \left(0.0002 \times 0.0004 m^2 \right)} = 12599 \frac{m}{kg}$$

$$\frac{\partial U_{LS}}{\partial A} = \frac{\dot{m}_L}{\rho_L A^2} = \frac{2.082 \times 10^{-6} \frac{kg}{s}}{992.08 \frac{kg}{m^3} \left(0.0002 \times 0.0004 \right)^2 m^4} = 327909.54 s^{-1} m^{-1}$$

so

$$\delta U_{LS} = \sqrt{\left(12599 \frac{m}{kg} \left(2.082 \times 10^{-9} \right) \frac{kg}{s} \right)^2 + \left(\left(327909.54 \right) s^{-1} m^{-1} \left(8.246 \times 10^{-9} \right) m^2 \right)^2}$$

$$\delta U_{LS} = \pm 2.704 \times 10^{-3} m/s$$

$$\frac{\delta U_{LS}}{U_{LS}} \times 100 = \frac{\pm 2.704 \times 10^{-3}}{2.745 \times 10^{-2}} \times 100 = 9.85\%$$

3. The uncertainty of frictional pressure drop $\left(\delta\left(\frac{dP}{dz}\right)_{friction}\right)$

$$\left(\frac{dP}{dz}\right)_{friction}=\left(\frac{dP}{dz}\right)_{Total}-\left(\frac{dP}{dz}\right)_{acceleration}-\left(\frac{dP}{dz}\right)_{c/e}$$

$$\left(\frac{dP}{dz}\right)_{Total}=368750\frac{Pa}{m}$$

$$\left(\frac{dP}{dz}\right)_{Acceleration}=G^2\left[\left(\frac{x^2}{\rho_G\alpha}+\frac{(1-x)^2}{(1-\alpha)\rho_L}\right)_{outlet}-\left(\frac{x^2}{\rho_G\alpha}+\frac{(1-x)^2}{(1-\alpha)\rho_L}\right)_{inlet}\right]$$

$$\left(\frac{dP}{dz}\right)_{Acceleration}$$

$$=\frac{(27.23)^2}{0.05}\left[\left(\frac{0.0444^2}{(1.0957)(0.976)}+\frac{(1-0.0444)^2}{(1-0.976)998.09}\right)-\left(\frac{0.0444^2}{1.167(0.976)}+\frac{(1-0.0444)^2}{(1-0.976)988.09}\right)\right]$$

$$=5.8439\frac{Pa}{m}$$

$$\left(\frac{dP}{dz}\right)_{friction}=362561\frac{Pa}{m}$$

$$\delta\left(\frac{dP}{dz}\right)_{friction}=\sqrt{\left(\delta\left(\frac{dP}{dz}\right)_{Total}\right)^2+\left(\delta\left(\frac{dP}{dz}\right)_{acceleration}\right)^2}$$

$$\delta\left(\frac{dP}{dz}\right)_{Total}=\pm737.5\frac{Pa}{m}$$

$$\delta\left(\frac{dP}{dz}\right)_{acceleration}=\sqrt{\left(\frac{\partial\left(\frac{dP}{dz}\right)_{acceleration}}{\partial x}\delta x\right)^2+\left(\frac{\partial\left(\frac{dP}{dz}\right)_{acceleration}}{\partial \alpha}\delta \alpha\right)^2}$$

$$x=\frac{G_g}{G}$$

$$\frac{\partial x}{\partial G}=\frac{G_g}{G^2}=\frac{1.21}{27.23^2}=1.632\times10^{-3}$$

$$\frac{\partial x}{\partial G_g}=\frac{1}{G^1}=\frac{1}{27.23}=3.672\times10^{-2}$$

$$\delta x=\sqrt{\left(\frac{\partial x}{\partial G}\delta G\right)^2+\left(\frac{\partial x}{\partial G_g}\delta G_g\right)^2}$$

The uncertainty of two-phase mass flux (δG)

$$G_g = \frac{\dot{m}_G}{A}$$

$$\delta G_g = \sqrt{\left(\frac{\partial G_g}{\partial \dot{m}_G}\delta \dot{m}_G\right)^2 + \left(\frac{\partial G_g}{\partial A}\delta A\right)^2}$$

$$\frac{\partial G_g}{\partial \dot{m}_G} = \frac{1}{A} = \frac{1}{\left(8\times10^{-8}\right)} = 1.25\times10^{7}\, m^{-1}$$

$$\frac{\partial G_g}{\partial A} = \frac{\dot{m}_g}{A^2} = \frac{9.67\times10^{-8}}{\left(8\times10^{-8}\right)^2} = 1.51\times10^{7}\,\frac{kg}{sm^4}$$

$$\delta G_g = \sqrt{\left(\left(1.25\times10^{7}\, m^{-1}\right)\left(7.733\times10^{-9}\,\frac{kg}{s}\right)\right)^2 + \left(\left(1.51\times10^{7}\,\frac{kg}{sm^4}\right)\left(8.246\times10^{-9}\, m^2\right)\right)^2} = 0.1576\,\frac{kg}{m^2 s}$$

$$G = \frac{\dot{m}_L + \dot{m}_G}{A}$$

$$\delta G = \sqrt{\left(\frac{\partial G}{\partial \dot{m}_L}\delta \dot{m}_L\right)^2 + \left(\frac{\partial G}{\partial \dot{m}_G}\delta \dot{m}_G\right)^2 + \left(\frac{\partial G}{\partial A}\delta A\right)^2}$$

$$\frac{\partial G}{\partial \dot{m}_L} = \left(\frac{\dot{m}_L + \dot{m}_G}{A}\right)\frac{1}{\dot{m}_L} = \left(\frac{\left(\left(2.08\times10^{-6}\right) + \left(9.667\times10^{-8}\right)\right)}{8\times10^{-8}}\right)\frac{1}{\left(2.08\times10^{-6}\right)} = 13080949.5\, m^2$$

$$\frac{\partial G}{\partial \dot{m}_G} = \left(\frac{\dot{m}_L + \dot{m}_G}{A}\right)\frac{1}{\dot{m}_G} = \left(\frac{\left(\left(2.08\times10^{-6}\right) + \left(9.667\times10^{-8}\right)\right)}{8\times10^{-8}}\right)\frac{1}{\left(9.667\times10^{-8}\right)} = 281456242.9\, m^2$$

$$\frac{\partial G}{\partial A} = \left(\frac{\dot{m}_L + \dot{m}_G}{A^2}\right) = \left(\frac{\left(\left(2.08\times10^{-6}\right) + \left(9.667\times10^{-8}\right)\right)}{\left(8\times10^{-8}\right)^2}\right) = 340104687.5\,\frac{kg}{m^4 s}$$

$$\delta G = \sqrt{\left(\left(13080949.5 m^2\right)\left(2.082\times10^{-9}\,\frac{kg}{s}\right)\right)^2 + \left(\left(281456242.9 m^2\right)\left(7.733\times10^{-9}\,\frac{kg}{s}\right)\right)^2 + \left(\left(340104687.5\,\frac{kg}{m^4 s}\right)\left(8.246\times10^{-9}\, m^2\right)\right)^2}$$

$$\delta G = \pm 3.5499\,\frac{kg}{ms}$$

$$\frac{\delta G}{G}\times100 = \frac{\pm3.5499}{27.3}\times100 = 13\%$$

The uncertainty of gas quality (δx)

$$\delta x = \sqrt{\left(\frac{\partial x}{\partial G}\delta G\right)^2 + \left(\frac{\partial x}{\partial G_g}\delta G_g\right)^2}$$

$$\delta x = \sqrt{\left(\left(1.632\times10^{-3}\right)\left(3.5499\right)\right)^2 + \left(\left(3.672\times10^{-2}\right)\left(0.1576\right)\right)^2} = \pm 8.189\times10^{-3}$$

The uncertainty of void fraction $(\delta\alpha)$

$$\alpha = \frac{1}{1+\frac{(1-x)}{x}\left(\frac{\rho_G}{\rho_L}\right)^{\frac{2}{3}}} = 0.9760$$

$$\frac{\partial\alpha}{\partial x} = \left(\frac{1}{1+\frac{(1-x)}{x}\left(\frac{\rho_G}{\rho_L}\right)^{\frac{2}{3}}}\right)\frac{1}{x} = \left(\frac{1}{1+\frac{(1-0.0444)}{0.0444}\left(\frac{1.167}{995}\right)^{\frac{2}{3}}}\right)\frac{1}{0.0444} = 18.17$$

$$\delta\alpha = \sqrt{\left(\frac{\partial\alpha}{\partial x}\delta x\right)^2} = \sqrt{\left(\left(18.17\right)\left(\pm 8.189\times10^{-3}\right)\right)^2} = \pm 0.1488$$

$$\frac{\delta\alpha}{\alpha}\times 100 = \frac{\pm 0.14879}{0.976}\times 100 = 15.24\%$$

The uncertainty of accelerational pressure drop

$$\delta\left(\frac{dP}{dz}\right)_{acceleration} = \sqrt{\left(\frac{\partial\left(\frac{dP}{dz}\right)_{acceleration}}{\partial x}\delta x\right)^2 + \left(\frac{\partial\left(\frac{dP}{dz}\right)_{acceleration}}{\partial\alpha}\delta\alpha\right)^2}$$

$$\frac{\partial\left(\frac{dP}{dz}\right)_{acceleration}}{\partial x} = \frac{G^2}{L}\left(\frac{-2+2x}{\rho_L(1-\alpha)} + \frac{2x}{\rho_G\alpha}\right) = \frac{27.24^2}{0.05}\left(\frac{-2+2(0.0444)}{995(1-0.976)} + \frac{2(0.0444)}{1.167(0.976)}\right) = -30.71$$

$$\frac{\partial\left(\frac{dP}{dz}\right)_{acceleration}}{\partial\alpha} = \frac{G^2}{L}\left(\frac{(1-x)^2}{\rho_L(1-\alpha)} - \frac{x^2}{\rho_G\alpha^2}\right) = \frac{27.24^2}{0.05}\left(\frac{(1-0.0444)^2}{995(1-0.976)} - \frac{0.0444^2}{1.167(0.976)}\right) = 541.8$$

$$\delta\left(\frac{dP}{dz}\right)_{acceleration} = \sqrt{\left(\left(-30.71\right)\left(\pm 8.189\times10^{-3}\right)\right)^2 + \left(\left(541.8\right)\left(\pm 0.1488\right)\right)^2} = \pm 80.62$$

4. The uncertainty of the friction factor (δf)

The uncertainty of two-phase Reynolds number

$$\mathrm{Re}_{TP} = \frac{GD_h}{\mu_{TP}}$$

$$\frac{\partial \mathrm{Re}_{TP}}{\partial G} = \frac{D_h}{\mu_{TP}} = \frac{0.0002667}{0.00059801} = 0.446$$

$$\frac{\partial \mathrm{Re}_{TP}}{\partial D_h} = \frac{G}{\mu_{TP}} = \frac{27.23}{0.00059801} = 45534.3$$

$$\delta \mathrm{Re}_{TP} = \sqrt{\left(\frac{\partial \mathrm{Re}_{TP}}{\partial G}\delta G\right)^2 + \left(\frac{\partial \mathrm{Re}_{TP}}{\partial D_h}\delta D_h\right)^2}$$

The uncertainty of two-phase mass flux

$$\delta G = \pm 3.5499 \frac{kg}{ms}$$

$$\frac{\delta G}{G} \times 100 = \frac{\pm 3.5499}{27.3} \times 100 = 13\%$$

so the uncertainty of two-phase Reynolds number is

$$\delta \mathrm{Re}_{TP} = \sqrt{\left((0.446)(3.5499)\right)^2 + \left((45534.3)\left(8.246\times10^{-9}\right)\right)^2} = 1.583$$

$$\frac{\delta \mathrm{Re}_{TP}}{\mathrm{Re}_{TP}} \times 100 = \frac{\pm 1.583}{11.3845} \times 100 = 13.9\%$$

The uncertainty of the friction factor

$$\delta f = \sqrt{\left(\frac{\partial f}{\partial\left(\frac{dP}{dz}\right)_{friction}}\delta\left(\frac{dP}{dz}\right)_{friction}\right)^2 + \left(\frac{\partial f}{\partial \mathrm{Re}_{TP}}\delta \mathrm{Re}_{TP}\right)^2}$$

$$f = \left(\frac{dP}{dz}\right)_{frictional} \frac{\rho_L D_h^3}{2\,\mathrm{Re}_{TP}^2\,\mu_L^2} = 0.6842$$

$$\frac{\partial f}{\partial\left(\frac{dP}{dz}\right)_{friction}} = \frac{\rho_L D_h^3}{2\,\mathrm{Re}_{TP}^2\,\mu_L^2} = \frac{(983.18)(0.0002667)^3}{2(11.3845)^2\,(0.00064434)^2} = 1.733\times10^{-4}$$

$$\frac{\partial f}{\partial \mathrm{Re}_{TP}} = -\left(\frac{dP}{dz}\right)_{friction} \frac{\rho_L D_h^3}{\mathrm{Re}_{TP}^3\,\mu_L^2} = -\left(\frac{18128}{0.05}\right)\frac{(983.18)(0.0002667)^3}{(11.3845)^3\,(0.00064434)^2} = 11.038$$

$$\delta f = \sqrt{\left(\left(1.733\times10^{-4}\right)\delta\left(\frac{dP}{dz}\right)_{friction}\right)^2 + \left((11.038)(1.583)\right)^2}$$

5. The uncertainty of the Nusselt number (δNu)

The uncertainty of the heat transfer at the test section

$$\delta Q_{bulk} = \sqrt{\left(\frac{\partial Q_{bulk}}{\partial \dot{m}}.\delta \dot{m}\right)^2 + \left(\frac{\partial Q_{bulk}}{\partial T_{fluid,in}}.\delta T_{fluid,in}\right)^2 + \left(\frac{\partial Q_{bulk}}{\partial T_{fluid,out}}.\delta T_{fluid,out}\right)^2}$$

$$Q_{bulk} = \dot{m} C_p (T_{fluid,out} - T_{fluid,in})$$

$$Q_{bulk} = (2.179\times10^{-6})\frac{kg}{s}(3931.6)\frac{J}{kg^{\circ}C}(49.0861-29.4495)^{\circ}C = 0.1682W$$

$$\frac{\partial Q_{bulk}}{\partial \dot{m}} = C_p (T_{fluid,out} - T_{fluid,in}) = (3931.6)\frac{J}{kg^{\circ}C}(49.0861-29.4495)^{\circ}C = 77.2\frac{kJ}{kg}$$

$$\dot{m} = \dot{m}_G + \dot{m}_L$$

$$\frac{\partial \dot{m}}{\partial \dot{m}_G} = (\dot{m}_G + \dot{m}_L)\dot{m}_G = \left(\left(9.667\times10^{-8}\right)\frac{kg}{s} + \left(2.0822\times10^{-6}\right)\frac{kg}{s}\right)\left(9.667\times10^{-8}\right)\frac{kg}{s}$$

$$\frac{\partial \dot{m}}{\partial \dot{m}_G} = 22.11\times10^{-13}\frac{kg}{s}$$

$$\delta \dot{m}_G = 9.667\times10^{-6}\frac{kg}{s}(0.08) = 7.734\times10^{-7}\frac{kg}{s}$$

$$\frac{\partial \dot{m}}{\partial \dot{m}_L} = (\dot{m}_G + \dot{m}_L)\dot{m}_L = \left(\left(9.667\times10^{-8}\right)\frac{kg}{s} + \left(2.0822\times10^{-6}\right)\frac{kg}{s}\right)\left(2.0822\times10^{-6}\right)\frac{kg}{s}$$

$$\frac{\partial \dot{m}}{\partial \dot{m}_L} = 4.537\times10^{-12}\frac{kg}{s}$$

$$\delta \dot{m}_L = 2.082\times10^{-6}\frac{kg}{s}(0.001) = 2.082\times10^{-9}\frac{kg}{s}$$

$$\delta \dot{m} = \sqrt{\left(\frac{\partial \dot{m}}{\partial \dot{m}_G}.\delta m_G\right)^2 + \left(\frac{\partial \dot{m}}{\partial \dot{m}_L}.\delta m_L\right)^2}$$

$$\delta \dot{m} = \sqrt{\left(22.11\times10^{-13}\frac{kg}{s}7.734\times10^{-7}\frac{kg}{s}\right)^2 + \left(4.537\times10^{-12}\frac{kg}{s}2.082\times10^{-9}\frac{kg}{s}\right)^2}$$

$$\delta \dot{m} = \pm1.71\times10^{-18}\frac{kg}{s}$$

$$\frac{\partial Q_{bulk}}{\partial T_{fluid,in}} = \dot{m} C_p = (2.1788\times10^{-6} kg)(3931.6\frac{J}{kg^{\circ}C}) = 8.5661\times10^{-6}\frac{kJ}{s^{\circ}C}$$

$$\frac{\partial Q_{bulk}}{\partial T_{fluid,out}} = -\dot{m} C_p = -(2.1788\times10^{-6} kg)(3931.6\frac{J}{kg^{\circ}C}) = -8.5661\times10^{-6}\frac{kJ}{s^{\circ}C}$$

so

$$\delta Q_{bulk} = \sqrt{\left(77.2\frac{kJ}{kg}1.71\times10^{-18}\frac{kg}{s}\right)^2 + \left(8.5661\times10^{-6}\frac{kJ}{s^{\circ}C}0.5^{\circ}C\right)^2 + \left((-8.5661\times10^{-6})\frac{kJ}{s^{\circ}C}0.5^{\circ}C\right)^2}$$

$$\delta Q_{bulk} = \pm6.057\times10^{-6}\frac{kJ}{s} = \pm6.057\times10^{-6} kW$$

$$\frac{\delta Q_{bulk}}{Q}\times100 = \frac{\pm6.057\times10^{-6}}{0.0001682}\times100 = 3.6\%$$

The uncertainty of the heat flux $\left(\delta q^{"}\right)$

$$\delta q^{"} = \sqrt{\left(\frac{\partial q^{"}}{\partial Q_{bulk}}.\delta Q_{bulk}\right)^2 + \left(\frac{\partial q^{"}}{\partial L}.\delta L\right)^2 + \left(\frac{\partial q^{"}}{\partial H}.\delta H\right)^2 + \left(\frac{\partial q^{"}}{\partial W}.\delta W\right)^2}$$

$$q^{"} = \frac{Q_{bulk}}{A_b} = \frac{Q_{bulk}}{(2H+W)L} = \frac{0.1682W}{\left((2\times0.0002m)+0.0004m\right)(0.05m)} = 4.205\frac{kW}{m^2}$$

$$\frac{\partial q^{"}}{\partial Q_{bulk}} = \frac{1}{(2H+W)L} = \frac{1}{\left((2\times0.0002m)+0.0004m\right)(0.05m)} = 25000m^{-2}$$

$$\frac{\partial q^{"}}{\partial L} = \frac{Q_{bulk}}{(2H+W)L^2} = \frac{0.1682W}{\left((2\times0.0002m)+0.0004m\right)(0.05m)^2} = 84.1\frac{kW}{m^2}$$

$$\frac{\partial q^{"}}{\partial H} = \frac{Q_{bulk}}{(2H+W)LH} = \frac{0.1682W}{\left((2\times0.0002m)+0.0004m\right)(0.05m)(0.0002m)} = 21.025\frac{kW}{m^3}$$

$$\frac{\partial q^{"}}{\partial W} = \frac{Q_{bulk}}{(2H+W)LW} = \frac{0.1682W}{\left((2\times0.0002m)+0.0004m\right)(0.05m)(0.0004m)} = 10.5125\frac{kW}{m^3}$$

$$\delta Q_{bulk} = \pm6.057\times10^{-6} kW$$

$$\delta L = \left(0.05m\right)(0.05) = 2.5\times10^{-3} m$$

$$\delta H = \left(0.0002m\right)(0.05) = 1\times10^{-5} m$$

$$\delta W = (0.0004m)(0.05) = 2\times10^{-5} m$$

$$\delta q^{"} = \sqrt{\left(\left(25000m^{-2}\right)\left(\pm6.057\times10^{-6}kW\right)\right)^2 + \left(\left(84.1m^{-2}\right)\left(1\times10^{-5}m\right)\right)^2 + \left(\left(21.025m^{-3}\right)\left(1\times10^{-5}m\right)\right)^2 + \left(\left(10.5125m^{-3}\right)\left(2\times10^{-5}m\right)\right)^2}$$

$$\delta q^{"} = \pm0.3891\frac{kW}{m^2}$$

$$\frac{\delta q^{"}}{q^{"}} \times 100 = \frac{\pm 0.3891}{4.205} \times 100 = 9.25\%$$

The uncertainty of the wall temperature $\left(\delta T_{wall,avg}\right)$

$$T_{wall,avg} = \frac{1}{N} \sum_{i=1}^{N} T_i$$

$$\delta T_{wall,avg} = \sqrt{N\left(\frac{1}{N}\delta T\right)^2}$$

$$\delta T_{wall,avg} = \sqrt{5\left(\frac{1}{5}.(0.5)\right)^2}$$

$$\delta T_{wall,avg} = \pm 0.2236^{\circ} C$$

The uncertainty of the fluid temperature $\left(\delta T_{fluid}\right)$

$$T_{fluid} = \frac{T_{fluid,in} + T_{fluid,out}}{2}$$

$$\delta T_{fluid} = \sqrt{2\left(\frac{1}{2}.\left(0.5^{\circ} C\right)\right)^2}$$

$$\delta T_{fluid} = \pm 0.3536^{\circ} C$$

The uncertainty of the heat transfer coefficient $\left(\delta h\right)$

$$\delta h = \sqrt{\left(\frac{\partial h}{\partial T_{wall}}.\delta T_{wall}\right)^2 + \left(\frac{\partial h}{\partial T_{fluid}}.\delta T_{fluid}\right)^2 + \left(\frac{\partial h}{\partial q^{"}}.\delta q^{"}\right)^2}$$

$$h = \frac{q^{"}}{T_{wall} - T_{fluid}} = \frac{4.205 \frac{kW}{m^2}}{\left(75.08 - 39.27\right)^{\circ} C} = 0.1174 \frac{kW}{m^{2\,\circ} C}$$

$$\frac{\partial h}{\partial T_{wall}} = \frac{q^{"}}{\left(T_{wall} - T_{fluid}\right)T_{wall}} = \frac{4.205 \frac{kW}{m^2}}{\left(75.08 - 39.27\right)^{\circ} C \left(75.08\right)^{\circ} C} = 1.564 \times 10^{-3}$$

$$\frac{\partial h}{\partial T_{fluid}} = \frac{q^{"}}{\left(T_{wall} - T_{fluid}\right)T_{fluid}} = \frac{4.205 \frac{kW}{m^2}}{\left(75.08 - 39.27\right)^{\circ} C \left(39.27\right)^{\circ} C} = 2.99 \times 10^{-3}$$

$$\frac{\partial h}{\partial q^{"}} = \frac{1}{T_{wall} - T_{fluid}} = \frac{1}{(75.08 - 39.27)^{\circ} C} = 2.793 \times 10^{-2}$$

$$\delta h = \sqrt{\left((1.564 \times 10^{-3})(0.2236^{\circ})\right)^2 + \left((2.99 \times 10^{-3})(0.3536)\right)^2 + \left((2.793 \times 10^{-2})(0.3891)\right)^2}$$

$$\delta h = \pm 1.092 \times 10^{-2} \frac{kW}{m^2 {}^{\circ} C}$$

$$\frac{\delta h}{h} = \frac{\pm 1.092 \times 10^{-2} \frac{kW}{m^2 {}^{\circ} C}}{0.1174 \frac{kW}{m^2 {}^{\circ} C}} = 9.3\%$$

The uncertainty of the Nusselt number (δNu)

$$\delta Nu = \sqrt{\left(\frac{\partial Nu}{\partial h}.\delta h\right)^2 + \left(\frac{\partial Nu}{\partial D}.\delta D_h\right)^2}$$

$$Nu = \frac{hD_h}{k} = \frac{\left(0.1174 \frac{kW}{m^2 K}\right)(0.0002667m)}{0.00063157 \frac{kW}{m \cdot K}} = 0.04958$$

$$\frac{\partial Nu}{\partial h} = \frac{D_h}{k} = \frac{0.0002667m}{0.00063157 \frac{kW}{m \cdot K}} = 0.4223$$

$$\frac{\partial Nu}{\partial D_h} = \frac{h}{k} = \frac{0.1174 \frac{kW}{m^2 K}}{0.00063157 \frac{kW}{m \cdot K}} = 185.89$$

$$\delta Nu = \sqrt{\left((0.4223)(1.092 \times 10^{-2})\right)^2 + \left((185.89)(8.246 \times 10^{-9})\right)^2}$$

$$\delta Nu = \pm 4.612 \times 10^{-3}$$

$$\frac{\delta Nu}{Nu} = \frac{\pm 4.612 \times 10^{-3}}{0.04958} = 9.3\%$$

Table A. Uncertainties of measured quantities and calculated parameters conclusion

Variable	Maximum relative uncertainty	Source
Pressure	±0.2%	Manufacturers specs (Bourdon HEANI)
Temperature	±0.4%	Manufacturers specs (Omega)
Water mass flow rate	±0.1%	Resolution limit
Gas volumetric flow rate	±8%	Resolution limit
Channel dimension	±5%	Resolution limit
Superficial velocity of gas	±12.8%	Uncertainty Propogation (Figiola and Beasley, 2006 on eq. 14)
Superficial velocity of liquid	±9.85%	Uncertainty Propogation (Figiola and Beasley, 2006 on eq. 14)
Frictional pressure drop	±3.99%	Uncertainty Propogation (Figiola and Beasley, 2006 on eq. 14)
Nusselt number	±9.3%	Uncertainty Propogation (Figiola and Beasley, 2006 on eq. 14)

According to error analysis theory, the uncertainties in Table A. are estimated as follows (Figiota and Beasley, 2006).

APPENDIX B. GRAPHICAL PROGRAMMING FOR DATA ACQUISITION SYSTEM

The National Instrument data acquisition system is used to collect the experimental data which using NI LabVIEW software for the expermental computing and data visualization.

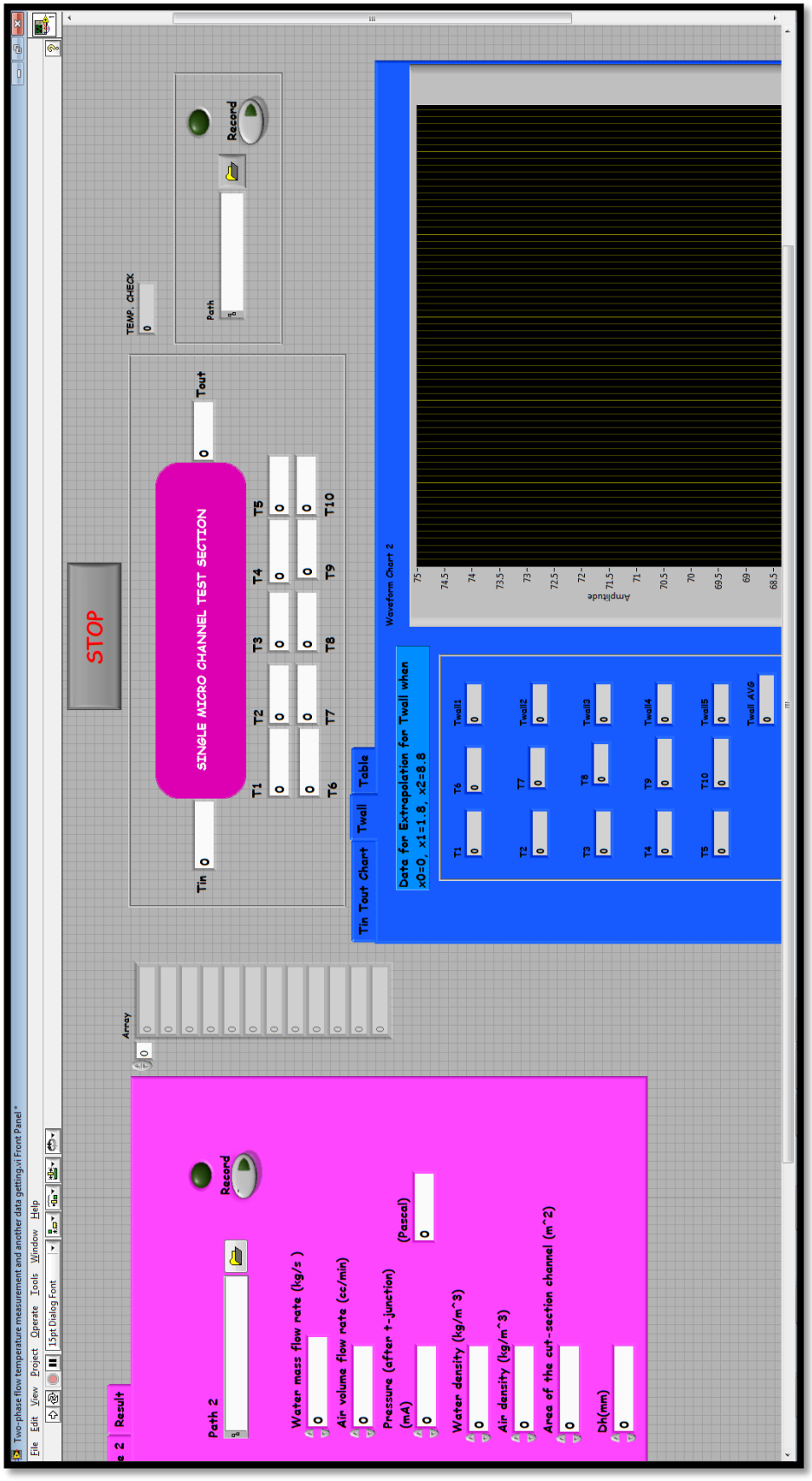

Figure B.1 LabVIEW front panel for monitoring and displaying the system

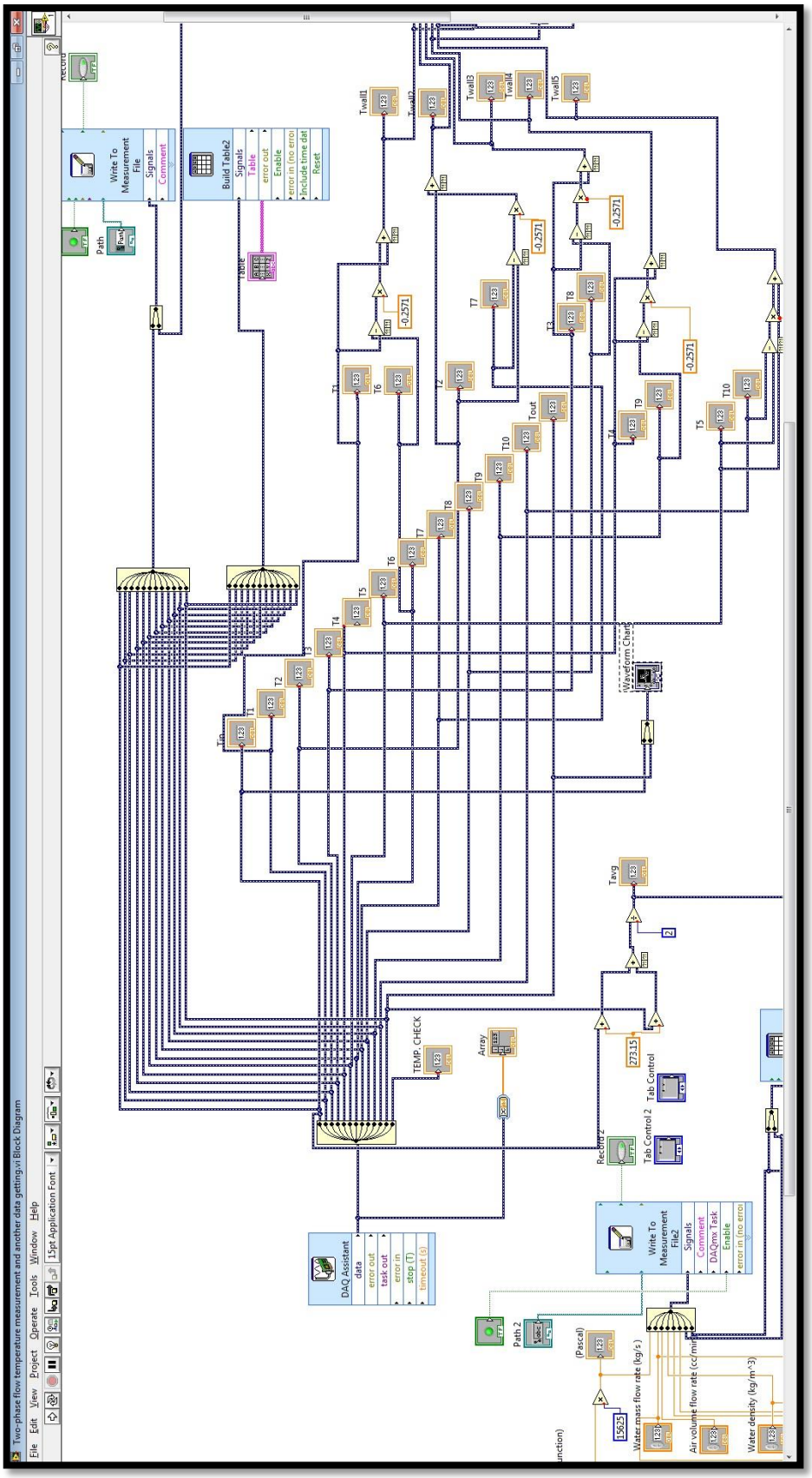

Figure B.2 The structure of a graphical block diagram

APPENDIX C. DRAWING CONSTRUCTIONS OF THE TEST SECTION ASSEMBLY

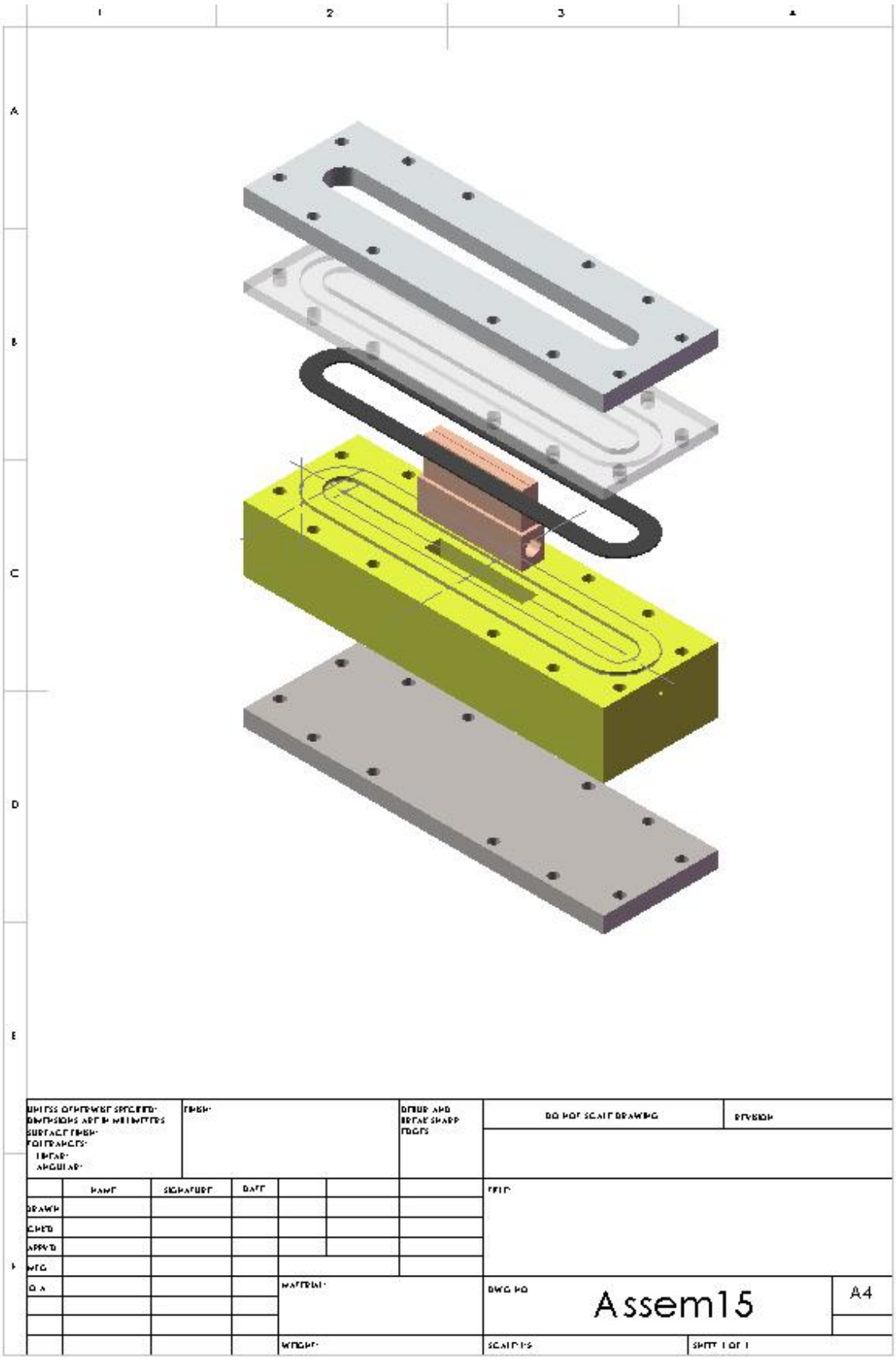

Figure C.1 The 2-D drawing of parts assembly

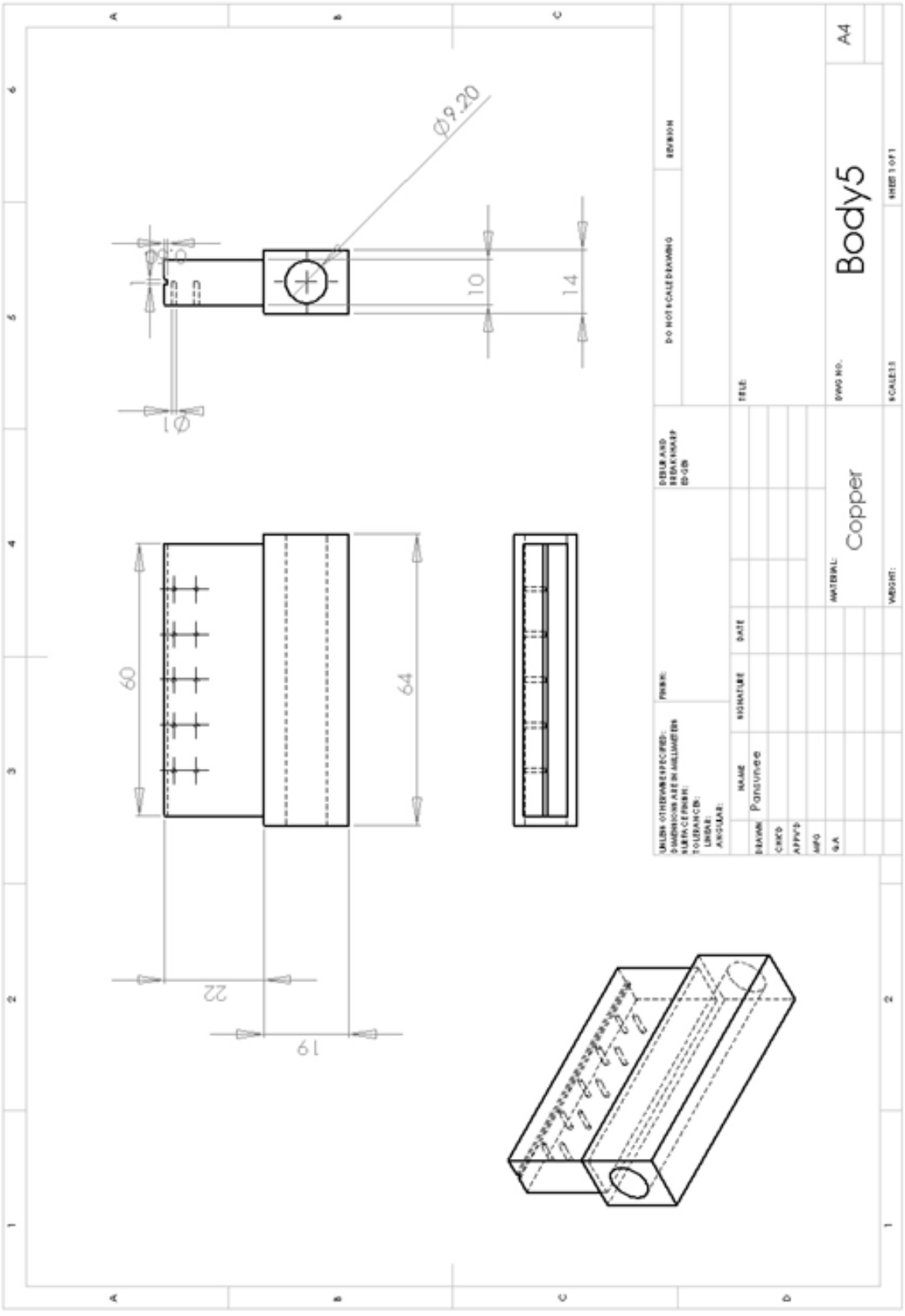

Figure C.2 The 2-D drawing of a copper body

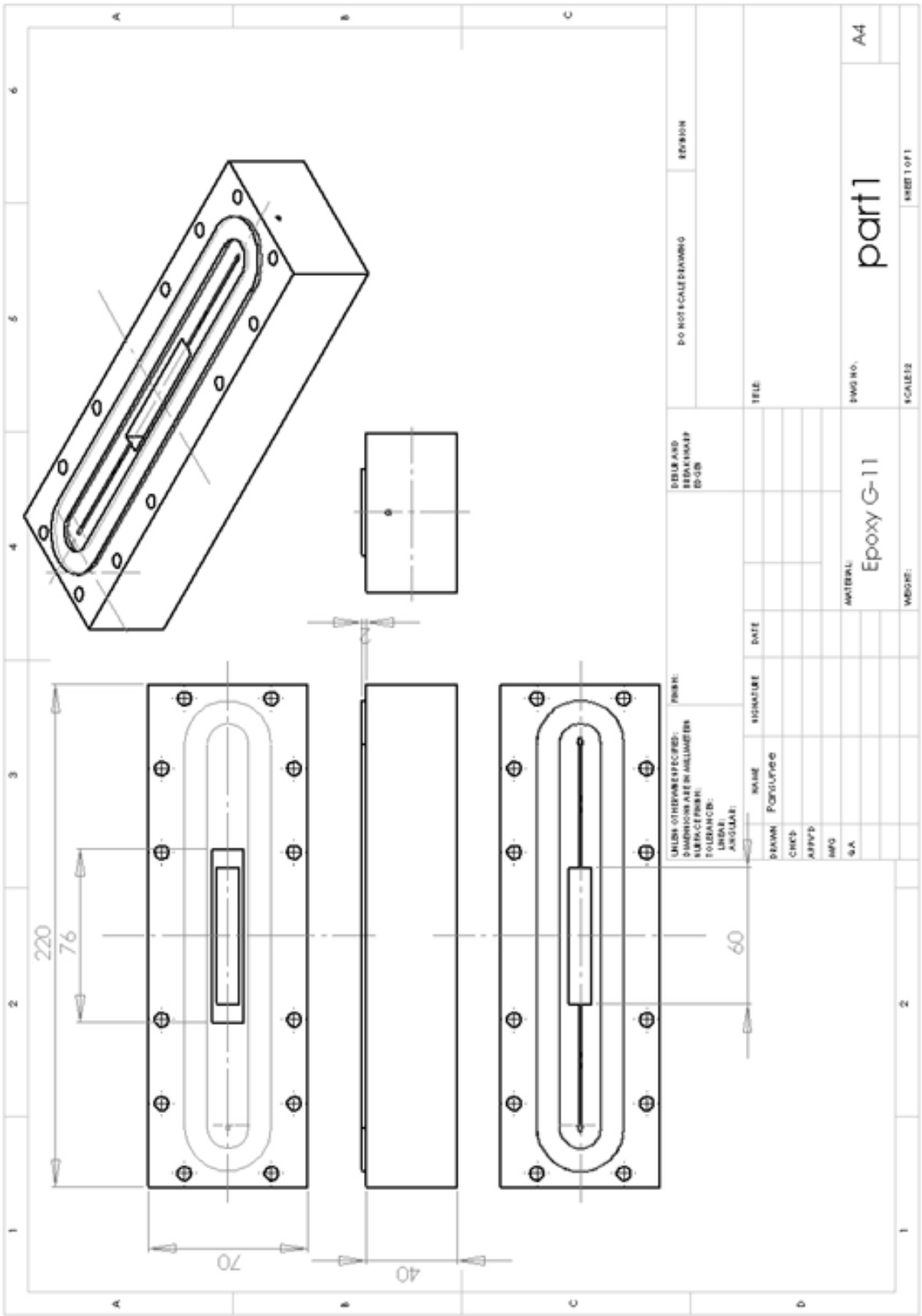

Figure C.3 The 2-D drawing of an insulator cover

CHAPTER 1 INTRODUCTION

1.1 Rational

The two-phase flow of gas and liquid is not only usually found in nature but is also widely used in energy and chemical applications. There are many related applications, such as oil transport and processing, steam generators, cooling systems, and reactors. Presently, the two-phase flow in microchannels has found applications as Micro-Electro-Mechanical Systems (MEMS), cooling electronics devices, medical systems, and bioengineering systems for the different purposes. Hence, the knowledge of fluid mechanics and heat transfer in micro scale devices is necessary. It leads to the study of the two-phase flow in microchannels with an emphasis on pressure drop, void fraction, flow pattern, and heat transfer coefficient. These are important elements for the design and development of devices to provide the best performance.

1.2 Literature review

Over the past decades, the single-phase flow of liquids or gases has been a topic of interest, and many questions about single-phase flow in small channels have been answer reasonably. On the other hand, the two-phase gas-liquid flow in microchannels has received comparatively little attention in literature (Fouilland and Fletcher, 2010).

For two-phase flow in the conventional size, gravitation highly influences the shear stress and surface tension. In microchannels, the influence of gravitation to shear stress and the surface tension relationship is reduced. This is a significant change of the various states discovered by Kreutzer et al. (2005) who proposed to divide the size of the channel. The flow pattern in the two phases with the critical Bond number can be used and has been analyzed by Bretherton (1961).

$$Bo = \frac{(\rho_L - \rho_G) g D_h^{\,2}}{\sigma} < 3.368 \tag{1.1}$$

where ρ_L and ρ_G are the gas and liquid densities, respectively, σ is the surface tension, g is the gravitational constant.

Thus, if we use air-water as the working fluid, it can be said that the hydraulic diameter of two-phase flow, which can be referred to as "microchannel," is $D_h < 5\,\text{mm}$.

Adiabatic Two-Phase Flow Patterns

During the past decade, there are a number of researches that study of two-phase flow pattern in microchannels. They conducted experiments by varying the shape, size, and working fluids of the microchannels for the purpose of observing the flow patterns and generating the flow regime maps.

Triplett et al. (1999) studied horizontal channels as circular microchannels with 1.1 and 1.45 mm diameter and semi-triangular microchannels with hydraulic diameters of 1.09 and 1.49 mm presented bubbly, churn, slug, slug-annular, and annular flow patterns. They found that the experimental data could be compared with the similar data of Suo and Griffith (1964) and Damianides and Westwater (1988).

For the vertical channels, Satitchaicharoen and Wongwises (2004) conducted the experiment to observe the two-phase flow of air-water, air-20 wt. % glycerol solution, and air-40 wt. % glycerol solution. They used five various sized rectangular test sections of mini-gap transparent acrylic glass channels and reported that the flow patterns of cap-bubbly, slug, churn, and annular types were observed in every size of channel, whereas the bubbly flow pattern was only found in the 40 mm × 3 mm rectangular section of air-water flow. The effects of channel sizes and working fluids were also discussed, which is consistent with the study of Zhao and Bi (2001). They reported that the bubbly flow was not found in the small channel.

There are various names of the same flow pattern that have been defined by many researchers, which results in the difficulty in distinguishing the same or different flow patterns. For example, slug (Triplett et al. 1999), Taylor (Yue et al. 2009), and bubble train flow patterns (Thulasidas et al. 1997) have been designed to indicate the same flow pattern.

Two-Phase Pressure Drop

Many researchers, such as Cubaud and Ho (2004), Chung and Kawaji (2004), and Saisorn and Wongwises (2008) have applied the separated flow model with the

modified two-phase frictional multiplier to predict a two-phase frictional pressure drop. On the other hand, Sur and Liu (2012) showed that using flow pattern-based model can predict the frictional pressure drop better than the separated or homogeneous flow model.

Heat Transfer Characteristics

Nowadays, electronic devices and the microprocessor are available in smaller sizes. The optimized cooling system design needs for heat transfer enhancement. Most researchers focus on the study of using flow boiling to enhance heat transfer in the system instead of on the single-phase flow that occur in low Nusselt number in the laminar flow condition. However, using flow boiling may be ineffective backflow, due to flashing, and instability phenomena. Moreover, it is not suitable to use air and water as the working fluids in flow boiling because of the high boiling temperature of the water. Thus, the segmented air-water flow in microchannels is proposed by Betz and Atinger (2010), Lim et al. (2013), and Majumder et al. (2013). They concluded that segmented air-water flow can enhance the Nusselt number in the channels up to 1.76 times over the single-phase flow of water. The factors that make the heat transfer enhancement are the mixer velocity from the air injection and the internal circulation of liquid slug induced by the gas bubbles, which enhances the mixing of the hot liquid film near the channel wall with cooler liquid from the center.

There are few researches on two-phase flow in microchannels, and reseaches on of the segmented flow characteristics in microchannels have gaps and conflicting conclusions as shown in Figure 1.1. Therefore, it is necessary to add to fill the research gap completely and accurately.

In this work, we performed the experimental study on two-phase flow patterns, the pressure drop, and segmented flow heat transfer characteristics of a rectangular microchannel having unique shape and size with different flow conditions in order to fulfill and improve the fundamental understanding of two-phase flow in the microchannel.

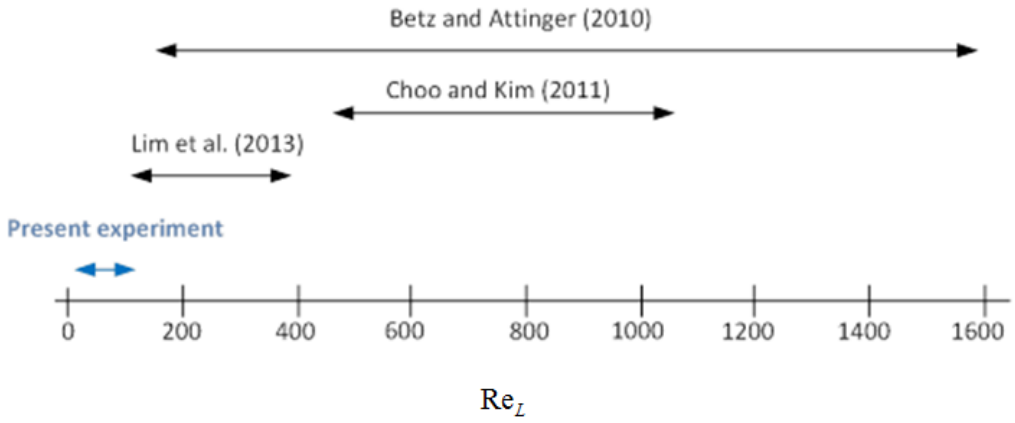

Figure 1.1 Range of Reynolds which the Nusselt number have been studied in the microchannels

1.3 Objectives

1. To conduct conduct systematic experiments to study on two-phase flow pattern, pressure drop and segmented flow heat transfer characteristics of a rectangular microchannel which has the unique shape, size and flowing conditions in order to fulfill and improve the fundamental understanding of two-phase flow in microchannels.

2. To compare the experimental results with the relevant models and correlations.

1.4 Scopes

1. A copper rectangular microchannel is used as the test section and placed horizontally.

2. Working fluids are air and water under ambient conditions.

3. Two-phase flow patterns, pressure drop and heat transfer characteristics will be determined.

CHAPTER 2 BACKGROUND KNOWLEDGE

2.1 Method of analysis

The method is used to analyze a two-phase flow, and is an extension of those already well known for single-phase flows. Three main types of assumption have been made. These are also applied to the flow in microchannel.

2.1.1 Homogeneous flow model

In this approach, the simplest approach to the problem, the two-phase flow is assumed to be a single-phase flow having pseudo-properties arrived by suitably weighting the properties of the individual phase.

2.1.2 Separated flow model

In this approach, the two phases of the flow are considered to be artificially segregated. Two sets of basic equations can now be written, one for each phase. Alternatively, the equations can be combined. In either case formation must be forthcoming about the area of the channel occupied by each phase (or alternatively, about the velocities of each phase) and about the friction interactions with the channel wall. In the former case additional information concerning the frictional interaction between phases is also required. This information is inserted into the basic equations, either from separating empirical relationships in which the void fraction and the wall shear stress relate to the primary variables, or on the basis of simplified models or flow.

2.1.3 Flow pattern model

In this more sophisticated approach the two-phase are considered to be arranged in one of three or four definite prescribed geometries. These geometries are based on the various configuration or flow patterns found when a gas and a liquid flow together in a channel. The basic equations are solved within the framework of each of these idealized representations. In order to apply these models, it is necessary to know when each should be used and to be able to predict the transition from one pattern to another. Nevertheless, this approach is still in its infancy.

2.2 Flow patterns

The particular flow pattern depends on the conditions of pressure, flow, heat flux and channel geometry. Each has a descriptive name and the design of a heat exchanger, it is desirable to know what the flow pattern or successive flow patterns are so that hydrodynamic or heat transfer theory appropriate to that pattern can be chosen.

2.2.1 Flow patterns in vertical co-current flow

The flow patterns encountered in vertical upwards co-current flow are shown schematically in Figure 2.1 together with actual photographs of each flow pattern.

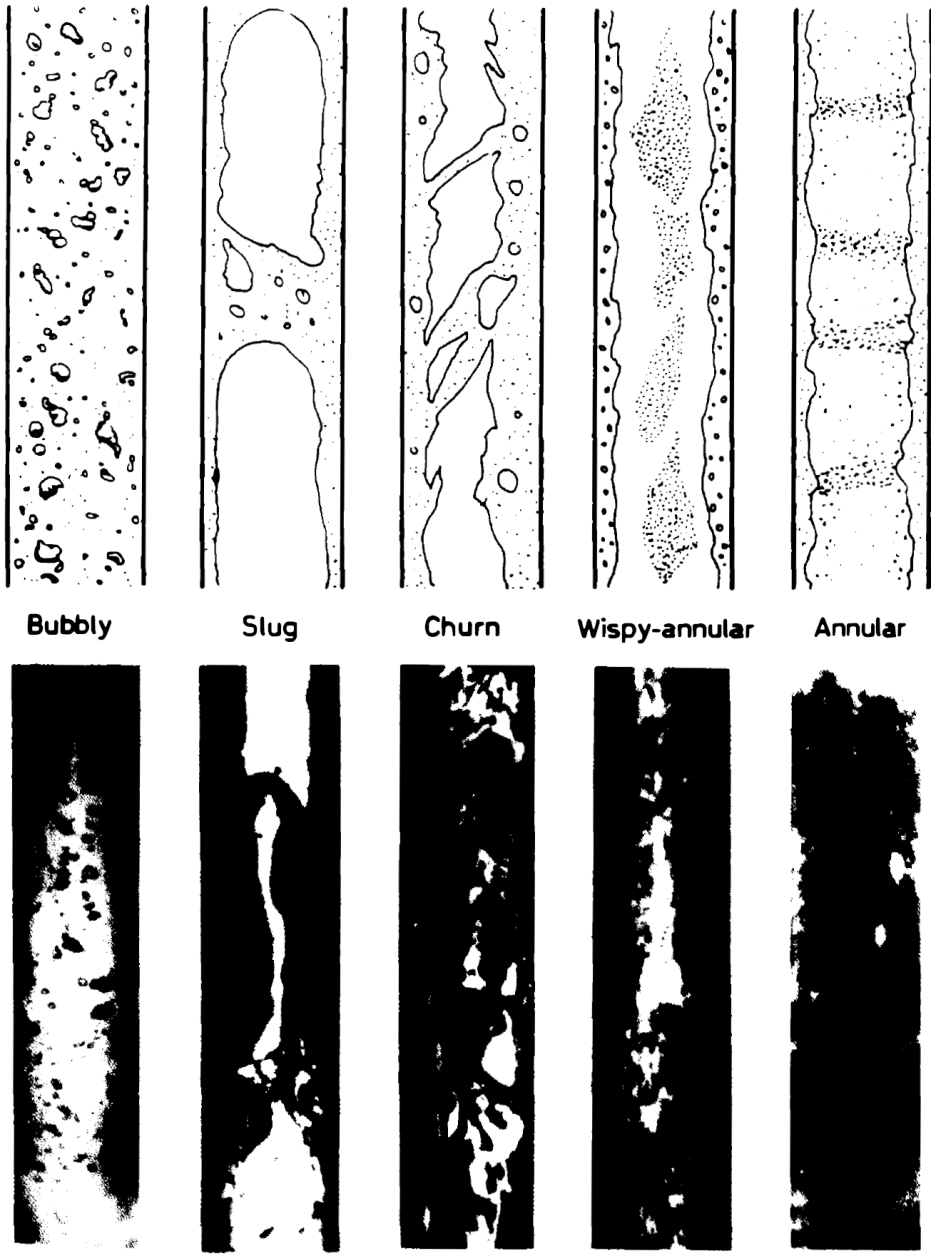

Figure 2.1 Flow patterns in vertical pipe (Collier and Thome, 1996)

2.2.1.1 Bubbly flow

In bubbly flow the gas or vapor phase is distributed as discrete bubbles in a continuous liquid phase. At one extreme the bubble may be large with a spherical cap and a flat tail. In this latter state, although the size of bubbles does not approach the diameter of the pipe, there may be some confusion with slug flow.

2.2.1.2 Slug flow

In slug flow, the gas or vapor bubbles are approximately the diameter of the pipe. The nose of the bubble has a characteristic spherical cap and a gas in the bubble is separated from the pipe wall by a slowly descending film of liquid. The liquid flow is contained in liquid slugs which separate successive gas bubbles. These slugs may or may not contain smaller entrained gas bubbles carried in the wake of the large bubble. The length of the main gas bubble can vary considerably.

2.2.1.3 Churn flow

Churn flow is formed by the breakdown of the large vapor bubbles in slug flow. The gas or vapor flows in a more or less chaotic manner through the liquid which is mainly displaced to the channel wall. The flow has an oscillatory or time varying character;

hence, the descriptive name ‘churn’ flow. This region is also sometimes referred to as semi-annular or slug-annular flow.

2.2.1.4 Wispy-annular flow

Wispy-annular flow has the form of a relatively thick liquid film on the walls of the pipe together with a considerable amount of liquid entrained in a central gas or vapor core. The liquid in the film is aerated by small gas bubbles and the entrained liquid phase appears as large droplets which have agglomerated into long irregular filaments or wisps.

2.2.1.5 Annular Flow

In annular flow, a liquid film forms at the pipe wall with a continuous central gas or vapor core.

2.2.2 Flow pattern in vertical heated channels

The formation of a two-phase mixture by vapor generation in a vertical heated tubular channel represents an important special case. The presence of a heat flux through the channel wall alters the flow pattern from that which would have occurred in a long unheated channel at the same local flow conditions. These changes occur due to two main reasons: firstly,the departure from thermodynamic equilibrium coupled with the presence of radial temperature profiles in the channel, and secondly, the departure from local hydrodynamic equilibrium throughout the channel. Figure 2.2 shows a schematic representation of a vertical tubular channel heated by uniform low heat flux and fed at its base with liquid just below the saturation temperature.

In the initial single-phase region, the liquid is being heated to the saturation temperature. A thermal boundary layer forms at the wall and a radial temperature profile is set up. At some position upstream, the wall temperature will exceed the saturation temperature and the conditions for the formation of vapor (nucleation) at the walls are satisfied. The vapor is formed at preferred positions or sites on the surface of the tube. Vapor bubbles gravity from these sites finally detach from tube wall to form a bubbly flow. With the production of more vapor, the bubble population increases with length and coalescence takes place to form slug flow, which in turn gives way to annular flow further along the channel. Close to the boiling point, the formation of

vapor at sites on the wall may cease and further vapor formation will be a result of evaporation at the liquid film-vapor core interface. Increasing velocities in the vapor core will cause entrainment of liquid in the form of droplets. The depletion of the liquid from the film by this entrainment and by evaporation finally causes the film to dry out completely. Droplets continue to exist and slowly evaporate until only single-phase vapor is present.

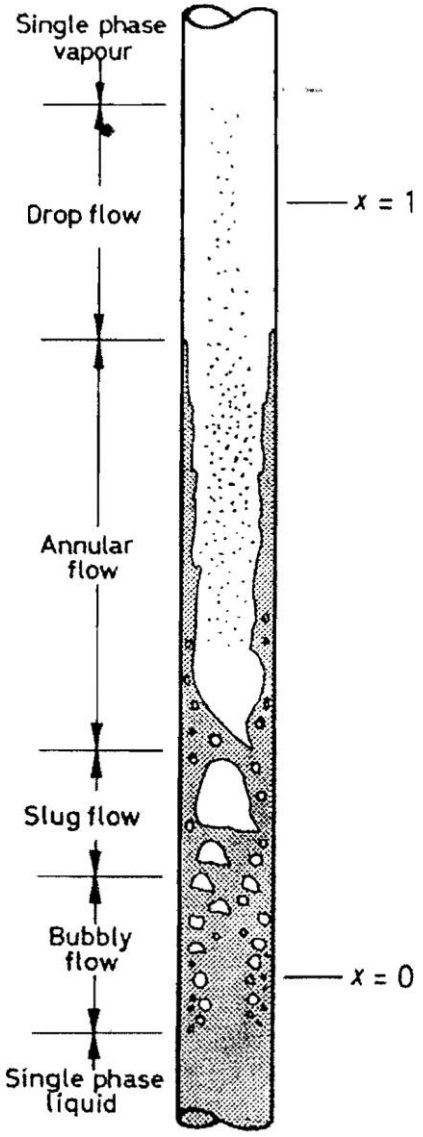

Figure 2.2 Flow patterns of flow boiling in vertical pipe (Collier and Thome, 1996)

2.2.3 Flow patterns in horizontal co-current flow

The flow patterns observed in co-current two-phase flow in horizontal and inclined tubular channels are complicated by asymmetry of the phases resulting from the influence of gravity. The generally accepted flow patterns as given by Alves (1954) are shown diagrammatically in Figure 2.3.

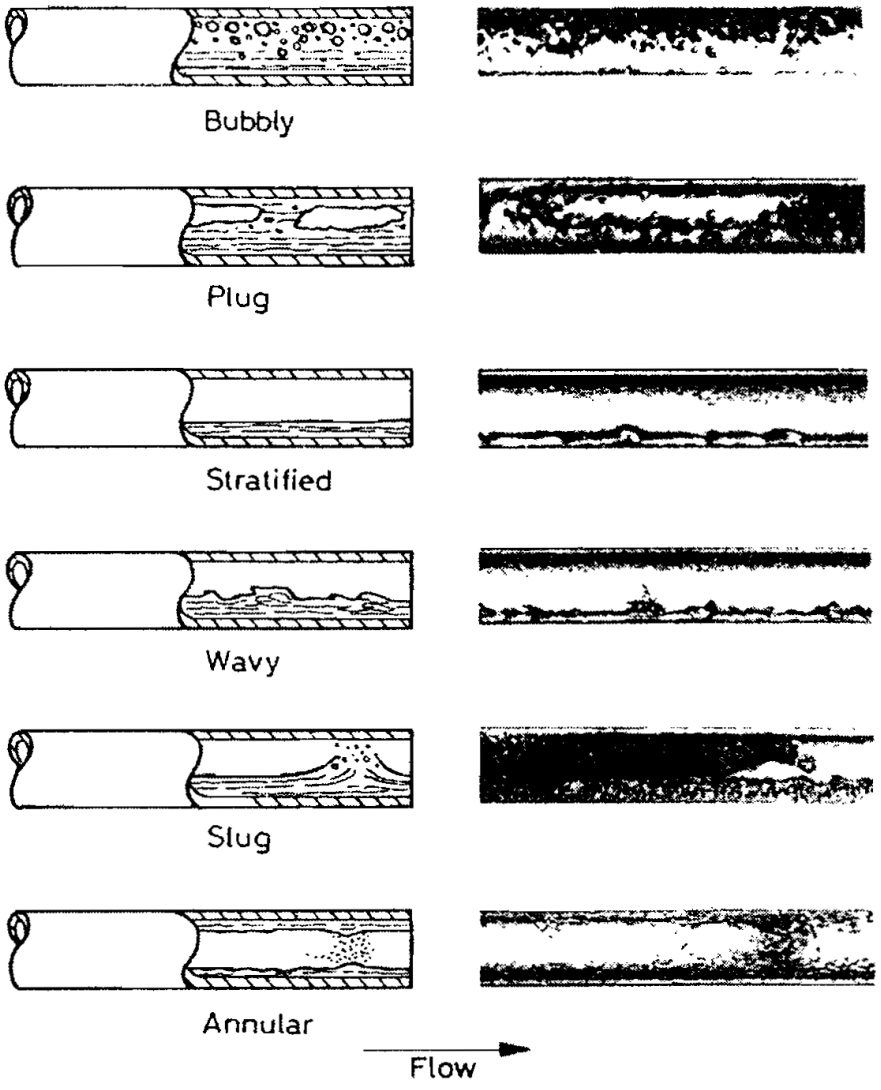

Figure 2.3 Flow patterns in horizontal pipe (Collier and Thome, 1996)

2.2.3.1 Bubbly flow

This flow pattern is similar to that in vertical flow except that the vapor bubbles tend to travel in the upper half of the pipe.

2.2.3.2 Plug flow

This is similar to slug flow in the vertical direction. Again the gas bubbles tend to travel in the upper half of the pipe.

2.2.3.3 Stratified flow

This pattern only occurs at very low liquid and vapor velocities. The two-phase flow separately with a relatively smooth interface.

2.2.3.4 Wavy flow

As the vapor velocity is increased the interface becomes disturbed by waves traveling in the direction of flow.

2.2.3.5 Slug flow

A further increase in vapor velocity causes the wave at the interface to be picked up to form a frothy slug which is propagated along the channel at a high velocity. The upper surface of the tube behind the wave is wetted by a residual film which drains into the bulk of the liquid.

2.2.3.6 Annular flow

A still higher vapor velocity will result in the information of a gas core with a liquid film around the periphery of the pipe. The film may or may not be continuous around the entire circumference but it will be thicker at the base of the pipe.

2.2.4 Flow patterns in horizontal heated channels

Similar flow structures previously discussed can also be found in the horizontal pipe. Flow patterns formed during the generation of vapor in horizontal tubular channels are influenced by departures from thermodynamic and hydrodynamic equilibrium in the same way as for vertical flow. Figure 2.4 shows a schematic representation of a horizontal tubular channel heated by a uniform low heat flux a fed with liquid just below the saturation temperature.

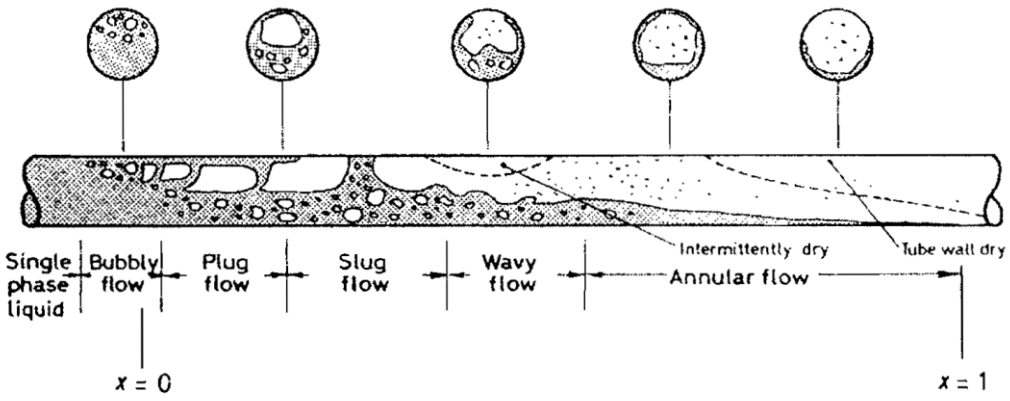

Figure 2.4 Flow patterns of flow boiling on horizontal pipe (Collier and Thome, 1996)

The design of many heat exchangers using horizontal tubular elements requires that these elements be interconnected using 180° return bends to form a serpentine

arrangement. In this case the influence of the return bend on the flow pattern is considerable. This topic is interesting for further research.

2.3 Hydrodynamic of segmented flow

Many researchers have preferred as the segmented gas-liquid flow stream as Taylor plug flow. Examples of gas-liquid and liquid-liquid segmented flow are shown in Figure 2.5

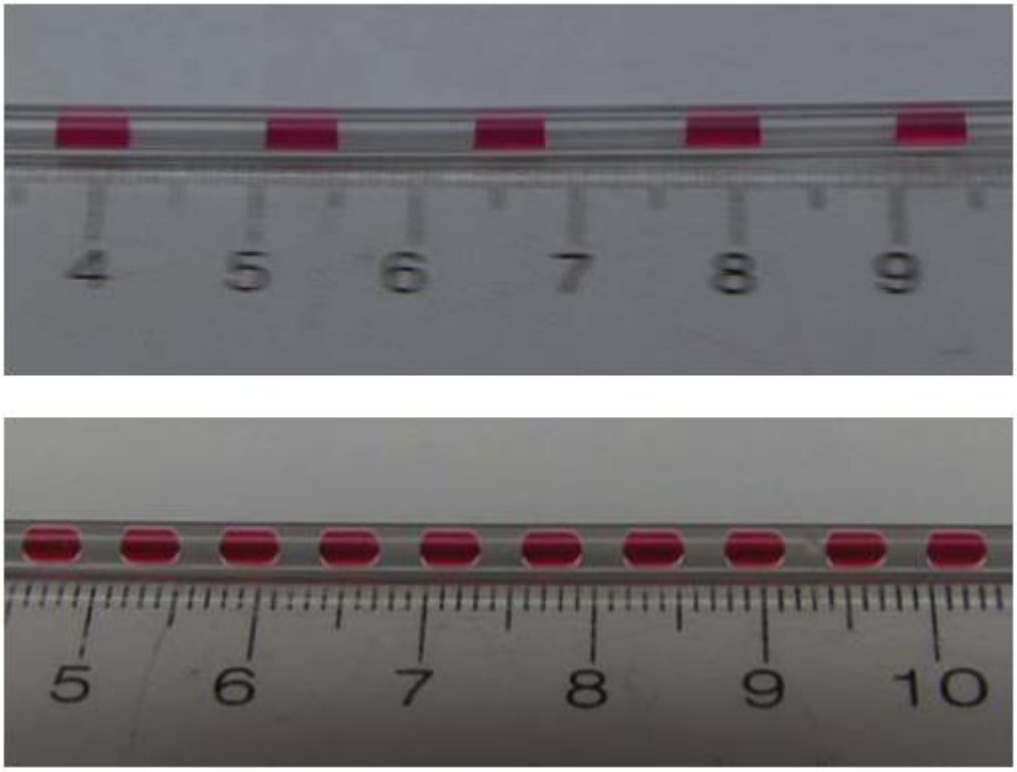

Figure 2.5 Water/air (top) and oil/water (bottom) segmented flow. The water has been tinted red for enhanced visualization of the interface (Janes et al., 2010)

An important characteristic of Taylor flow is presence of a pair of recirculation zones within the liquid plugs as shown in Figure 2.6. These zones result from the presence of the liquid/gas or liquid/liquid interface. The dynamics of the fluid motion is such that the circulation rolls in a manner akin of tank tracks in the direction of the flow. The circulation affects the flow in a manner which promotes radial transport of heat or mass in addition to a boundary layer renewal, since the fresh fluid is constantly being transported to the leading edge of the plug. In Muzychka et al. (2009), the authors show that heat transfer data for isothermal tubes scaled according to plug length so that the classic Graetz-Leveque model could be used as predictive measure of the thermal performance, provided curtain conditions are met.

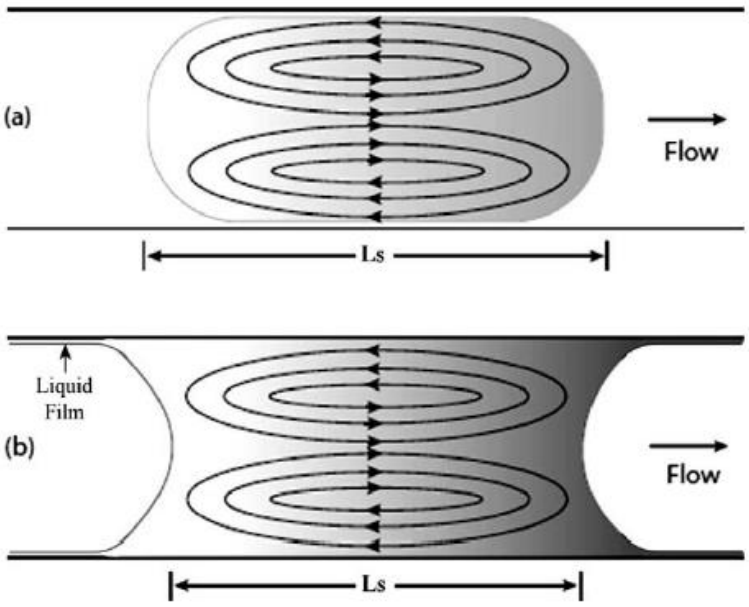

Figure 2.6 Liquid plug circulation in segmented flow; a) hydrophobic and b) hydrophilic (Talimi et al., 2012)

CHAPTER 3 EXPERIMENTAL APPARATUS

The schematic diagram of the test apparatus is shown in Fig. 3.1. Water and air were mixed by the Valco Tee connecter as Fig. 3.3 (SS, 0.25 mm bore, 1/16", 10-32) where the water was pumped from a peristaltic pump (Masterflex L/S, easy-load model 7518-00) and the mass flow rate of water was found by measuring at the outlet with a digital balance (320 ± 0.001 g). The air was injected to generate bubbles by air compressor through a pressure regulator and the air flow rates are measured by two sets of rotameter within the range of 5-50 sccm and 0.05-0.5 SCFH, respectively (Dwyer, 5-50 sccm ±8% uncertainty, 0.05-0.5 SCFH ±4% uncertainty. The pressure was varied depending on the mass flow rate. The pressure drop along the channel was measured (BOURDON HAENNI, type E913, 250 kPa, ± 0.5 kPa uncertainty). Thermocouples (Type T 0.5 mm diameter, Omega, 100 ms response time, ±0. 5°C or 0.4% uncertainty) are used to measure water temperatures at the inlet and outlet of the test section. The data of temperature and pressure were collected by a data acquisition system (National Instrument NI CompactDAQ).

A rectangular microchannel (Fig. 3.2) device consists of a single rectangular microchannel. It was made from a copper slab with the dimensions 500 mm of length, 400 μm of width, 200 μm of height. This 267 μm hydraulic diameter of microchannel used to create and observe the flow. The cover of the test section is transparent polycarbonate. The copper heat substrate was heated in the constant value by the cartridge heater from DC power supply source which verify the surface temperature by using the five rows of two thermocouples and calculate surface temperature by the linear extrapolation. The test section was good insulated by G10 epoxy and bolt together with the a copper part of rectangular microchannel and the aluminium cover plate to firm the assembly.

The flow was illuminated by the cold light (LED) source and stereo zoom microscope (Nikon SMZ745T) mounted together with a camera system (Nikon D7100, shutter speeds of 1/30 – 1/8,000 sec.) were used for record each flow pattern that occurred in a microchannel.

The experiments were conducted at the room temperature (30° C) at various air and liquid flow rates to define the flow regime maps. The system was allowed to approach steady conditions before the air and water flow rates, flow pattern and pressure drop were recorded.

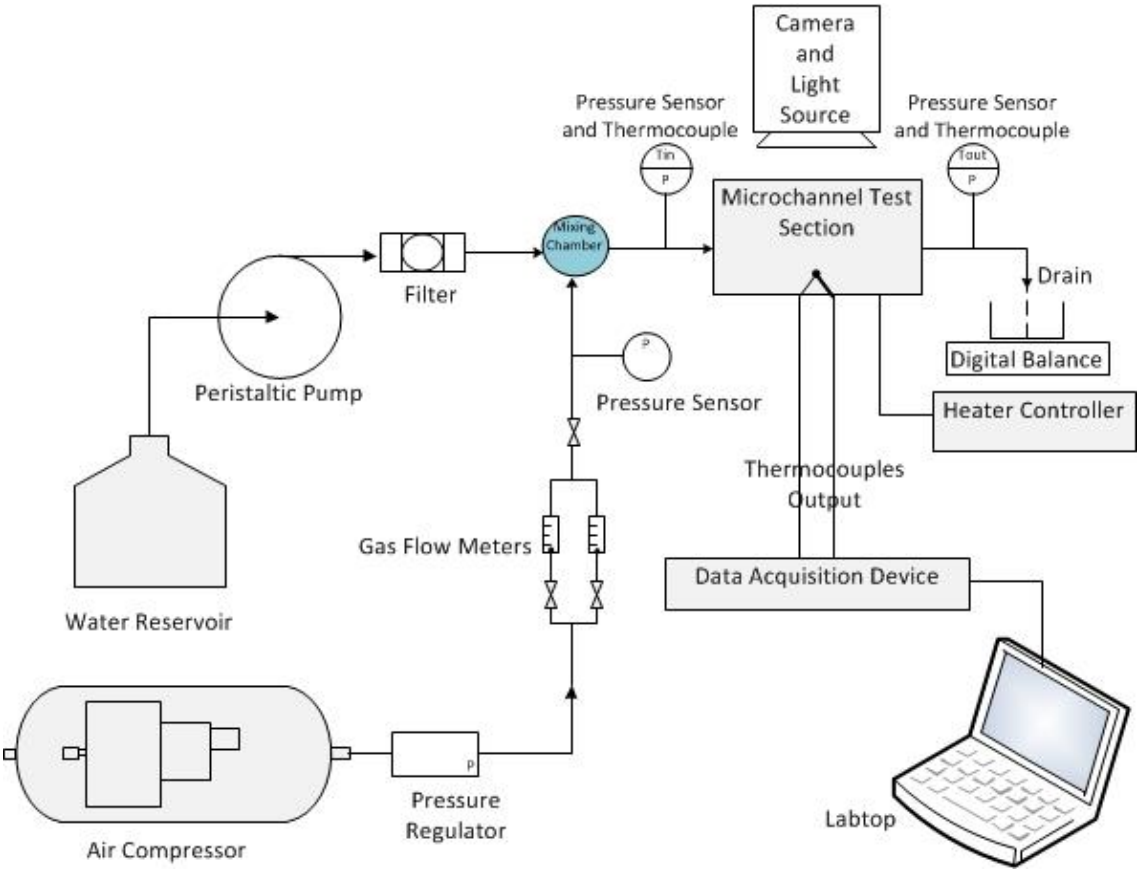

Figure 3.1 Schematic diagram of the experimental apparatus

3.1 Test Section

A rectangular microchannel (Fig. 3.2) device consists of a single rectangular microchannel. It was made from a copper slab with the dimensions 500 mm of length, 400 µm of width, 200 µm of height. This 267 µm hydraulic diameter of microchannel used to create and observe the flow. The cover of the test section is transparent polycarbonate. The copper heat substrate was heated in the constant value by the cartridge heater from DC power supply source which verify the surface temperature by using the five rows of two thermocouples and calculate the surface temperature by the linear extrapolation. The test section was good insulated by G10 epoxy and bolt together with the a copper part of rectangular microchannel and the aluminium cover plate to firm the assembly.

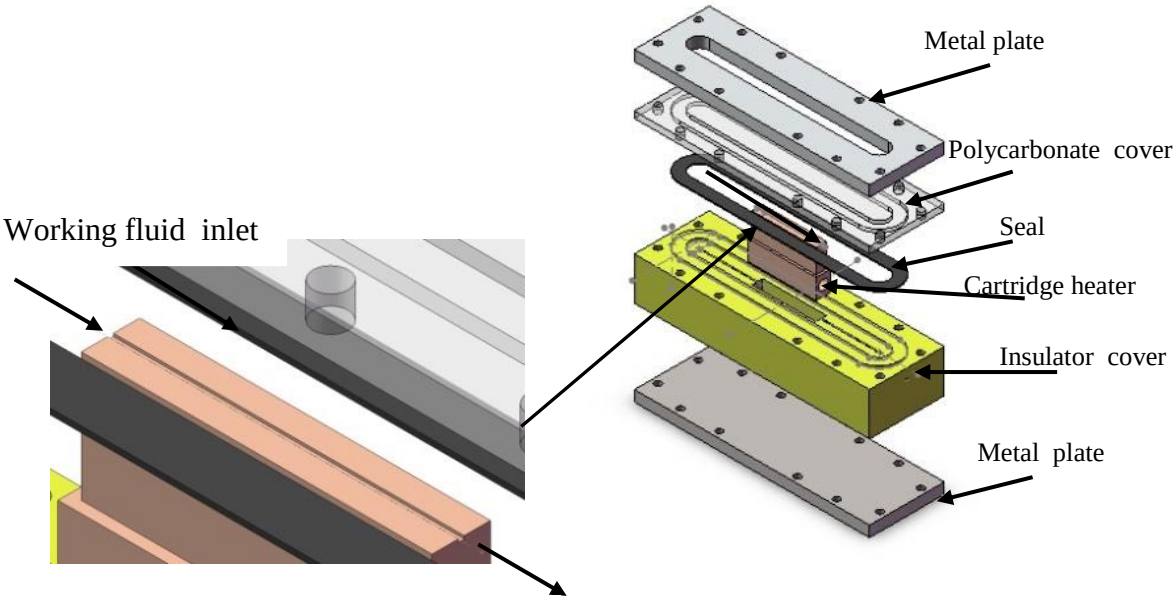

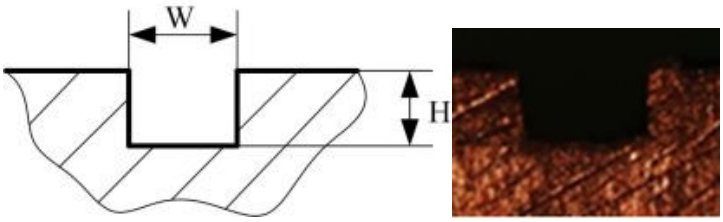

Section detail of microchannel after mixing section, W = 400 µm, H = 200 µm

Figure 3.2 test section

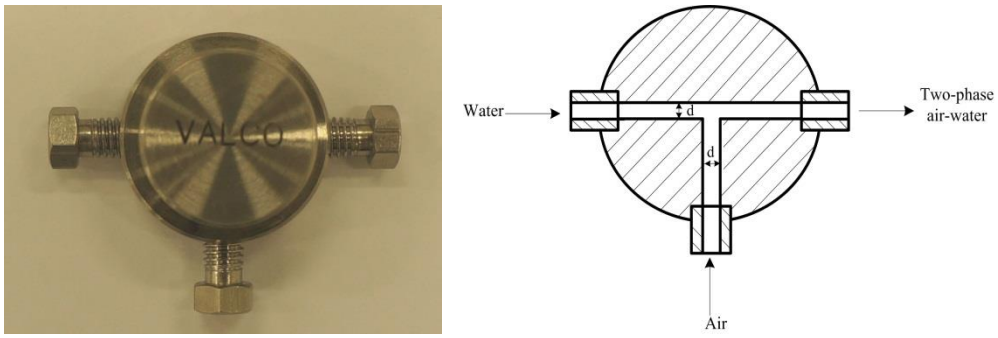

Figure 3.3 (a) Sketch and (b) actual photograph of the Valco Tee two-phase mixing chamber with d = 250 µm inner diameter.

Table 3.1 Uncertainties of measured quantities and calculated parameters

Variable	Maximum relative uncertainty
Pressure	±0.2%
Temperature	±0.4%
Heat flux	±3.6%
Water mass flow rate	±0.1%
Gas volumetric flow rate	±8%
Channel dimension	±5%
Superficial velocity of gas	±12.8%
Superficial velocity of liquid	±9.85%
Frictional pressure drop	±3.99%
Nusselt number	±9.3%

$$W_E = \sqrt{\left(\frac{dE}{dy_1} w_1\right)^2 + \left(\frac{dE}{dy_2} w_2\right)^2 + \ldots + \left(\frac{dE}{dy_n} w_n\right)^2} \quad (3.1)$$

where W is the error associated with any calculated parameter E

w is the error associated with any calculated parameter y

Kline and McClintock (1953)

CHAPTER 4 DATA REDUCTION

The following calculation is employed to determine the superficial velocities of the flow patterns, heat transfer coefficient, Nusselt number and two-phase friction factor, from the data recorded during each test run at steady state conditions.

4.1 Flow regime map

The use of multiple rotameters for the air and digital balance for water over the ranges of gas superficial velocities = 1.04-8.30 m/s of air and liquid superficial velocities = 0.0013-0.3429 m/s of water is defined as

$$U_{GS} = \frac{V_G}{A_{ch}} \tag{4.1}$$

$$U_{LS} = \frac{V_L}{A_{ch}} \tag{4.2}$$

where A_{ch} is the microchannel cross-sectional area, V_G and V_L are the volume flow rates of air and water are respectively.

4.2 Pressure drop

The pressure drop of fluid flow through a horizontal channel can be calculated from

$$\left(\frac{dP}{dz}\right)_{frictional} = f\,\frac{L}{D_h}\frac{U^2}{2g} \tag{4.3}$$

where f is friction factor, L is length of the channel test section, U is average velocity in the channel test section

The Reynolds number of gas, Re_G and liquid, Re_L are defined by

$$\mathrm{Re}_G = \frac{\rho_G U_{GS} D_h}{\mu_G},\ \mathrm{Re}_L = \frac{\rho_L U_{LS} D_h}{\mu_L} \tag{4.4}$$

where μ_G is the dynamic viscosity of gas and μ_L is the dynamic viscosity of liquid. Shah and London (1978) proposed a correlation of $f\,\mathrm{Re}$ for single-phase isothermal, incompressible and fully developed laminar flow in rectangular channel is

$$f\,\mathrm{Re} = 96(1 - 1.3553AR + 1.9467AR^2 - 1.7012AR^3 + 0.9564AR^4 - 0.2537AR^5) \tag{4.5}$$

$$AR = \frac{H}{W} \tag{4.6}$$

In this study, the experimentally derived friction factor is a function of Reynolds number for a rectangular channel with the aspect ratio AR =0.5 is

$$f = \frac{62.2}{\mathrm{Re}} \tag{4.7}$$

two-phase mixture can be treated as a single-phase fluid. A two-phase pressure drop consists of frictional, accelerational and gravitational terms (Carey (1992)). The gravitational terms are neglected in the horizontal flow study so, the formula is

$$\left(\frac{dP}{dz}\right)_{TP} = \left(\frac{dP}{dz}\right)_{friction} + \left(\frac{dP}{dz}\right)_{acceleration} + \left(\frac{dP}{dz}\right)_{c/e} \tag{4.8}$$

where

$\left(\frac{dP}{dz}\right)_{friction}$ is the frictional pressure drop, $\left(\frac{dP}{dz}\right)_{acceleration}$ is accelerational pressure drop and

$\left(\frac{dP}{dz}\right)_{c/e}$ represents pressure drop due to sudden contraction and expansion. All the components can be evaluated by the following expressions.

$$\left(\frac{dP}{dz}\right)_{friction} = f_{TP}\frac{1}{D_h}\frac{G^2}{2\rho_{TP}} \tag{4.9}$$

where f_{TP} is a two-phase friction factor, G is the mass flux and ρ_{TP} is the two-phase density

$$\rho_{TP} = \left(\frac{x}{\rho_G} + \frac{1-x}{\rho_L}\right)^{-1} \tag{4.10}$$

$$f_{TP} = \frac{62.2}{\mathrm{Re}_{TP}} \tag{4.11}$$

$$\mathrm{Re}_{TP} = \frac{GD_h}{\mu_{TP}} \tag{4.12}$$

$$\left(\frac{dP}{dz}\right)_{acceleration} = G^2\left[\left(\frac{x^2}{\rho_G\alpha} + \frac{(1-x)^2}{(1-\alpha)\rho_L}\right)_{outlet} - \left(\frac{x^2}{\rho_G\alpha} + \frac{(1-x)^2}{(1-\alpha)\rho_L}\right)_{inlet}\right] \tag{4.13}$$

$$\left(\frac{dP}{dz}\right)_{contraction} = \frac{G^2}{2\rho_L}\left[\left(\frac{1}{C_c}-1\right)^2 + \left(1-\frac{1}{\gamma^2}\right)\right]\left[1+\left(\frac{\rho_L}{\rho_G}-1\right)x\right] \tag{4.14}$$

$$\left(\frac{dP}{dz}\right)_{\exp ansion} = G^2\gamma(\gamma-1)\left[\frac{1-x^2}{\rho_L(1-\alpha)} + \frac{x^2}{\alpha\rho_G}\right] \tag{4.15}$$

x represents the mass quality, α is the void fraction, G is the mass velocity, C_c is the coefficient of contraction which can be given by Chisholm (1983).

$$C_c = \frac{1}{0.639\left[1+\left(\frac{1}{\gamma}\right)\right]^{\frac{1}{2}}+1} \tag{4.16}$$

where γ represents the ratio of the cross-sectional flow area in the flow passage connected to the channel test section to that in the channel test section.

The void fraction is used for calculation of acceleration pressure drop. Armand correlation (Armand and Treschev (1946)) was chosen which is in reasonable agreement with Serizawa et al. (2002) and Zhao and Bi (2001)

$$\alpha = 0.833\beta \tag{4.17}$$

when β and α are gas volumetric ratio and void fraction respectively.

Homogeneous flow model (HFM)

The homogeneous flow model assumes that the gas and liquid phases are so well mixed that the two-phase mixture can be treated as a single-phase fluid.

Viscosity for homogeneous flow model;

McAdams et al. (1942):
$$\mu_{TP} = \left(\frac{x}{\mu_G} + \frac{1-x}{\mu_L}\right)^{-1} \tag{4.18}$$

Owen (1961): $$\mu_{TP} = \mu_L \tag{4.19}$$

Dukler et al. (1964): $$\mu_{TP} = \beta\mu_G + (1-\beta)\mu_L \tag{4.20}$$

Beattie and Whalley (1982): $$\mu_{TP} = \beta\mu_G + (1-\beta)(1+2.5\beta)\mu_L \tag{4.21}$$

Lin et al. (1991): $$\mu_{TP} = \frac{\mu_G\mu_L}{\mu_G + x^{1.4}(\mu_L - \mu_G)} \tag{4.22}$$

Awad and Muzychka (2008): $$\mu_{TP} = \mu_G \frac{2\mu_G + \mu_L - 2(\mu_G - \mu_L)(1-x)}{2\mu_G + \mu_L + (\mu_G - \mu_L)(1-x)} \tag{4.23}$$

Choi and Kim (2011) proposed the accuracy of model predictions which was assessed using the mean absolute error (MAE), expresses as a percentage.

$$MAE = \frac{1}{M}\sum\left[\frac{\left|\Delta P_{TP,pred} - \Delta P_{TP,\exp}\right|}{\Delta P_{TP,\exp}} \times 100\right] \tag{4.24}$$

where $\Delta P_{TP,pred}$ is the pressure drop obtained from predicted model, $\Delta P_{TP,\exp}$ is the pressure drop obtained from an experiment and M is the number of data,

Separated flow model

For separated flow assumption which was found to be good agreement with the experimental data, SFMs are based on the-two phase multiplier (ϕ), which is defined as

$$\phi_L^2 = \left(\frac{dP}{dz}\right)_{TP} \Big/ \left(\frac{dP}{dz}\right)_L \tag{4.25}$$

Lockhart and Martinelli (1949) suggested that ϕ_L^2 is a function of the Martinelli parameter

$$\phi_L^2 = 1 + \frac{C}{X_{vv}} + \frac{1}{X_{vv}^2} \tag{4.26}$$

Where X_{vv} is a parameter of a laminar liquid-laminar gas flow

$$X_{vv} = \left[\left(\frac{dp}{dz}\right)_L \Big/ \left(\frac{dp}{dz}\right)_G\right]^{0.5} = \left(\frac{1-x}{x}\right)^{0.5}\left(\frac{\rho_G}{\rho_L}\right)^{0.5}\left(\frac{\mu_L}{\mu_G}\right)^{0.5} \tag{4.27}$$

Friedel (1979) developed a correlation with 25,000 data points. The smallest pipe diameter used is 4 mm. The correlation includes the gravity effect through the Froude number (Fr), and the effects of surface tension and total mass flux using the Weber number (We). The correlation is the following form

$$\phi_L^2 = E + \frac{3.24FH}{Fr_H^{0.45} We_L^{0.035}} \tag{4.28}$$

The dimensionless factors Fr_H, F and H are as follows:

$$E = (1-x^2) + x^2 \frac{\rho_L f_G}{\rho_G f_L} \tag{4.29}$$

$$F = x^{0.78}(1-x)^{0.224} \tag{4.30}$$

$$H = \left(\frac{\rho_L}{\rho_G}\right)^{0.91} \left(\frac{\mu_G}{\mu_L}\right)^{0.19} \left(1-\frac{\mu_G}{\mu_L}\right)^{0.7} \tag{4.31}$$

The liquid Weber We_L is defined as:

$$We_L = \frac{GD_h}{\sigma \rho_H} \tag{4.32}$$

Using the following alternative definition of the homogeneous flow density ρ_H based on vapor quality:

$$\rho_H = \left(\frac{x}{\rho_G} + \frac{1-x}{\rho_L}\right)^{-1} \tag{4.33}$$

4.3 Heat Transfer Characteristics

The average Nusselt number for single phase and segmented flow was defined as:

$$Nu = \frac{hD_h}{k_L} \tag{4.34}$$

where h is heat transfer coefficient and k_L is the thermal conductivity of water. The value of heat flux and heat transfer coefficient are calculated as:

$$h = \frac{q^{"}}{T_{wall} - T_{fluid}} \tag{4.35}$$

$$q^{"} = \frac{Q_{Bulk}}{(2H + W)L} \tag{4.36}$$

where T_{wall} is the average wall temperature using linear extrapolation from five rows of two T-type thermocouples. T_{fluid} is the average value fluid temperature defined as

$$T_{fluid} = 0.5(T_{fluid,in} + T_{fluid,out}) \tag{4.37}$$

The total heat transfer to the fluid was determined from using a simple energy balance from inlet to exist:

$$Q_{bulk} = \dot{m} C_p (T_{f,out} - T_{f,in}) \tag{4.38}$$

The thermal equilibration of air and water in segmented flow allows the determination of the heat capacity as mass averaged properties.

$$C_p = \phi C_{p,water} + (1 - \phi) C_{p,air} \tag{4.39}$$

where the mass fraction of water is

$$\phi = \left(\frac{\rho_{water} Q_{water}}{\rho_{water} Q_{water} + \rho_{air} Q_{air}} \right) \tag{4.40}$$

ρ_{water} and ρ_{air} are the water and air densities respectively.

CHAPTER 5 RESULTS AND DISCUSSION

In this chapter, the results of adiabatic two-phase flow patterns, flow regime maps, frictional pressure drop and heat transfer characteristics are presented and discussed.

5.1 Adiabatic Two-phase flow patterns and flow pattern transitions

5.1.1 Flow patterns

Four different two-phase flow patterns were identified, namely, the segmented flow, throat-annular, throat-annular/liquid and annular flow as shown in Figure 5.1

a) Segmented Flow

This flow pattern features liquid slugs alternating with air bubbles. With the width of the bubbles close to the width of the channel, the length of the bubble would be longer than the hydraulic diameter of the channel. No water droplets were recognized in the air bubbles, nor are any air bubbles presents in the water slugs, as well. After all, segmented flow is also called plug, Taylor, slug, bubble-train, and intermittent flow.

b) Annular flow

In this study, annular flow was observed at the lowest range liquid superficial velocity U_{LS} and at the rising of gas superficial velocity U_{GS} respectively. The volume of liquid is flowing through the channel as thin film around the microchannel wall.

c) Throat-annular flow

Throat-annular flow, also known as the Taylor-annular, ring, slug-ring flow, and slug-annular flow is the flow pattern of the two consecutive bubbles coalescence. In this pattern, a gas core is surrounded by a liquid film where large-amplitude waves appear in the liquid film, small bubbles are sometimes presented in the liquid. These are considered to be the transition zone into the next flow pattern between the annular and slug-annular/liquid flow when the liquid phase rises to high velocities.

d) Throat-annular/ Liquid flow

This flow pattern is characterized by periodic oscillation between throat-annular flow and single phase liquid flow. It is observed when the ULS is higher, and the wave of the water throat-annular side wall reaches the wave of water film on the opposite side.

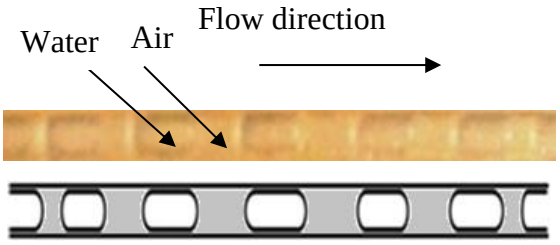

U_{GS} = 1.037 m/s, U_{LS} = 0.1257 m/s

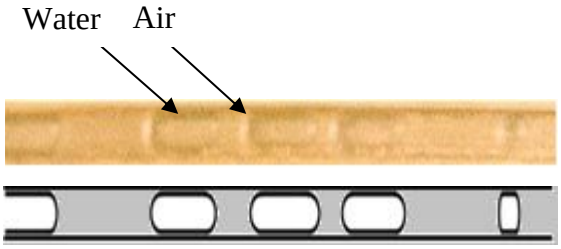

U_{GS} = 2.075 m/s, U_{LS} = 0.095 m/s

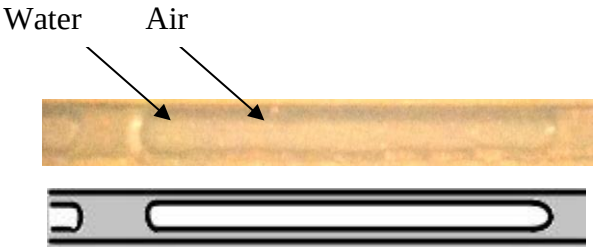

U_{GS} = 2.075 m/s, U_{LS} = 0.095 m/s

a) Segmented Flow

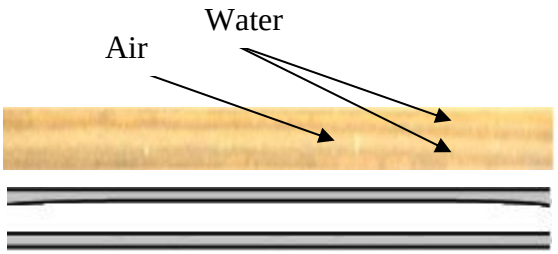

U_{GS} = 5.189 m/s, U_{LS} = 0.038 m/s

b) Annular Flow

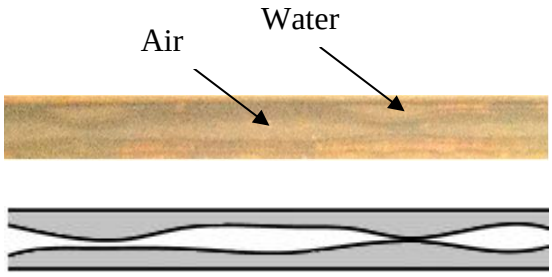

U_{GS} = 3.113 m/s , U_{LS} = 0.08865 m/s

c) Throat-annular flow

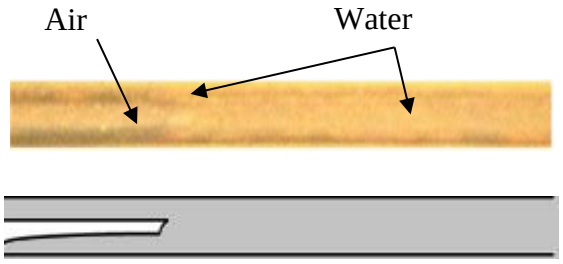

U_{GS} = 1.557 m/s, U_{LS} = 0.1118 m/s

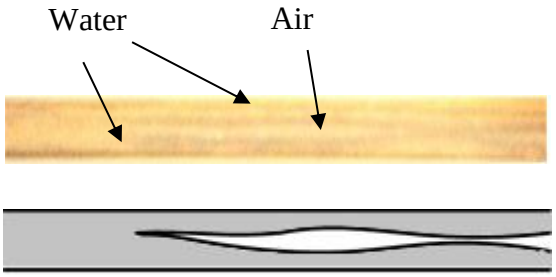

U_{GS} = 3.113 m/s, U_{LS} = 0.1796 m/s

d) Throat-Annular/Liquid Flow

Figure 5.1 Flow visualizations of two-phase air-water flow patterns in the 267 μm of hydraulic diameter rectangular microchannel test section

5.1.2 Flow regime maps

Illustrates the flow regime map of this experiment; using U_{GS} and U_{LS} as coordinates, we found that segmented flow occurred at the lowest range of U_{GS}. When the U_{GS} the rises, the bubble's size grows and expanded along the channel. This effect causes the reduction of the segmented flow pattern and then changes to another flow pattern as throat-annular, throat-annular/liquid, and annular flow up to the rates of U_{GS} and U_{LS}.

The flow regime maps in Figure 5.3 – Figure 5.8 were developed by Triplett et al. (1999), Kawahara et al. (2002), Qu et al. (2004), Waelchli and von Rohr (2006), Saisorn and Wongwises (2008), and Wang et al. (2012). The criteria used to select the flow maps are the similar channel dimensions and similar working fluids. In some of these previous studies, the segmented flow was categorized as slug or intermittent flow, the throat-annular is categorized as slug-annular or ring or ring-slug without distinction. For clarity, only the transition boundary lines are shown in the flow map results from the literature, and the individual flow regime is marked in the text accordingly.

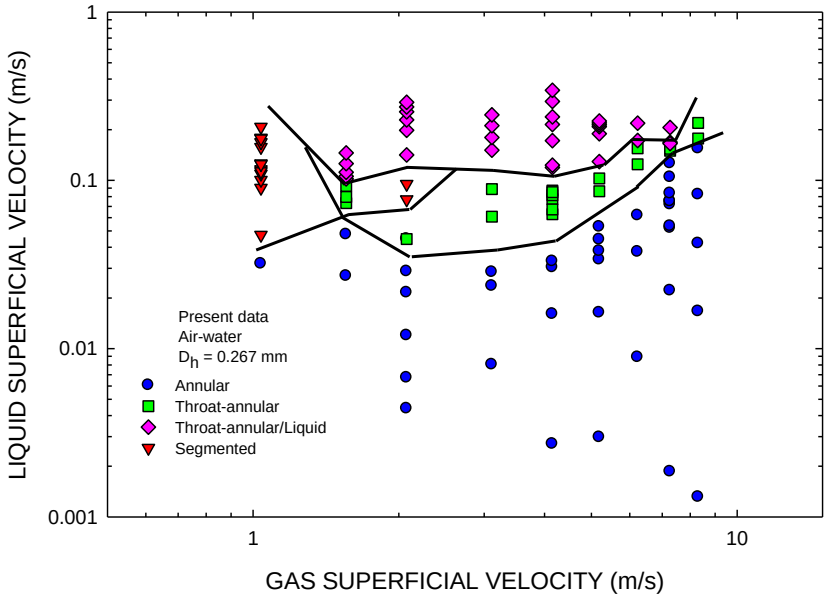

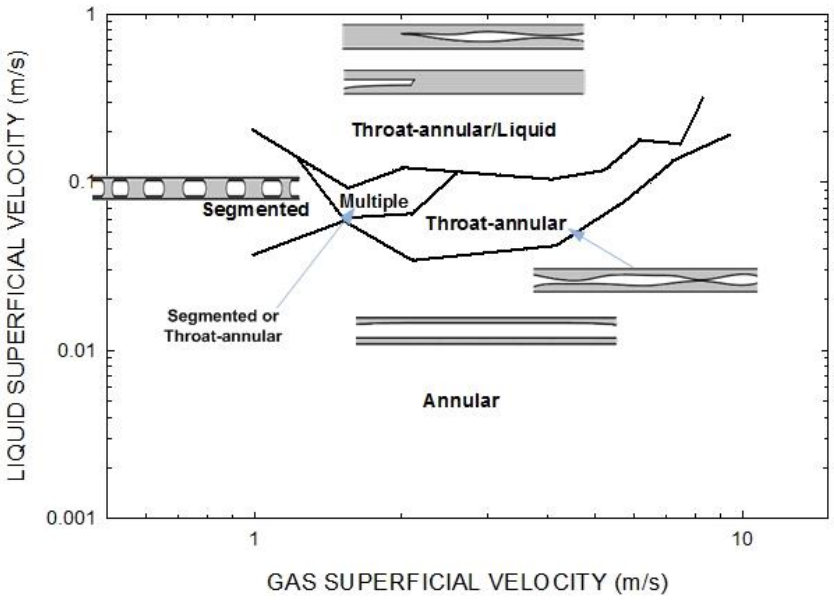

Figure 5.2 Two-phase flow pattern map for two-phase air-water flow through a 267 µm diameter channel

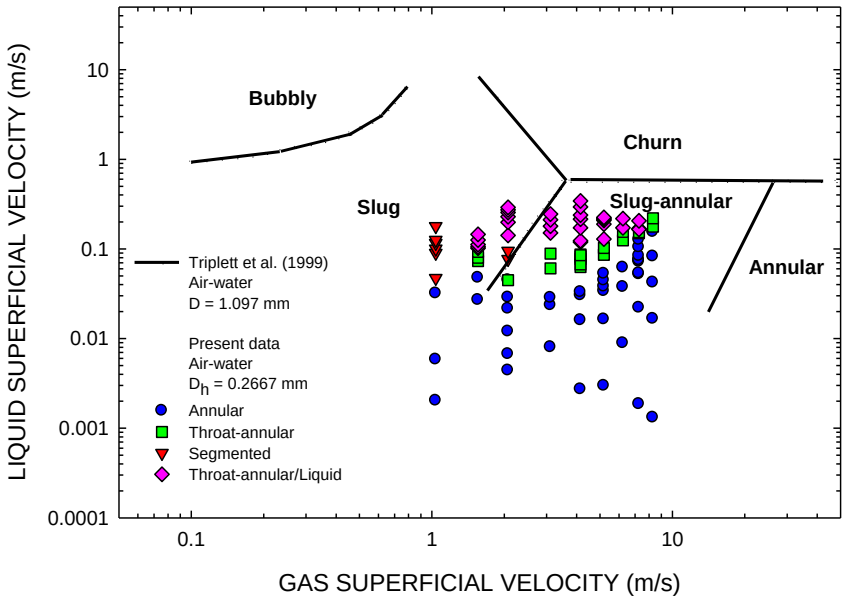

Figure 5.3 Comparison of the observed flow patterns with the transition lines by Triplett et al. (1999)

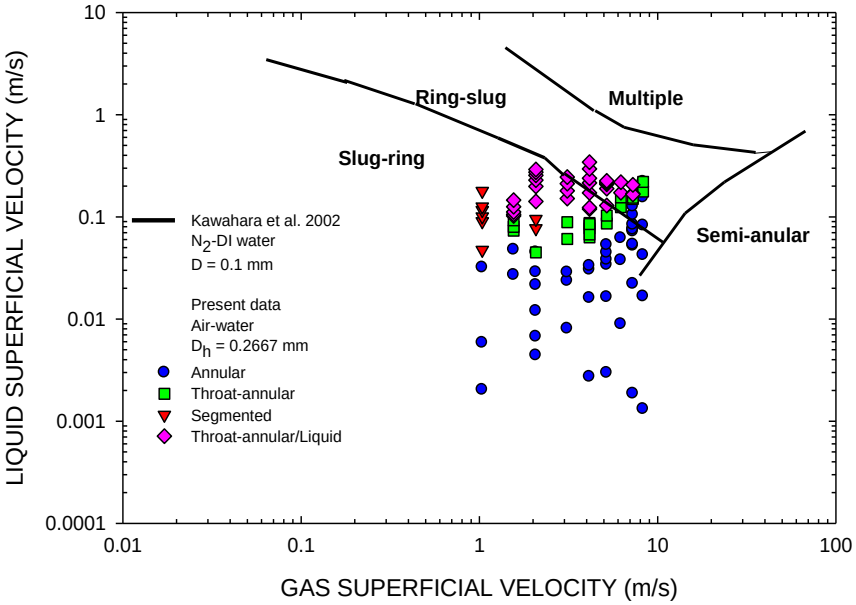

Figure 5.4 Comparison of the observed flow patterns with the transition lines by Kawahara et al. (2002)

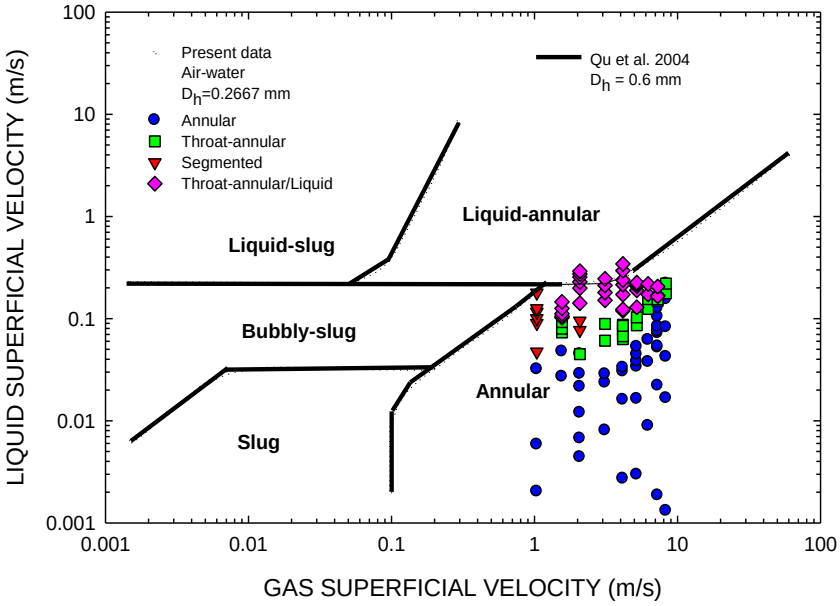

Figure 5.5 Comparison of the observed flow patterns with the transition lines by Qu et al. (2004)

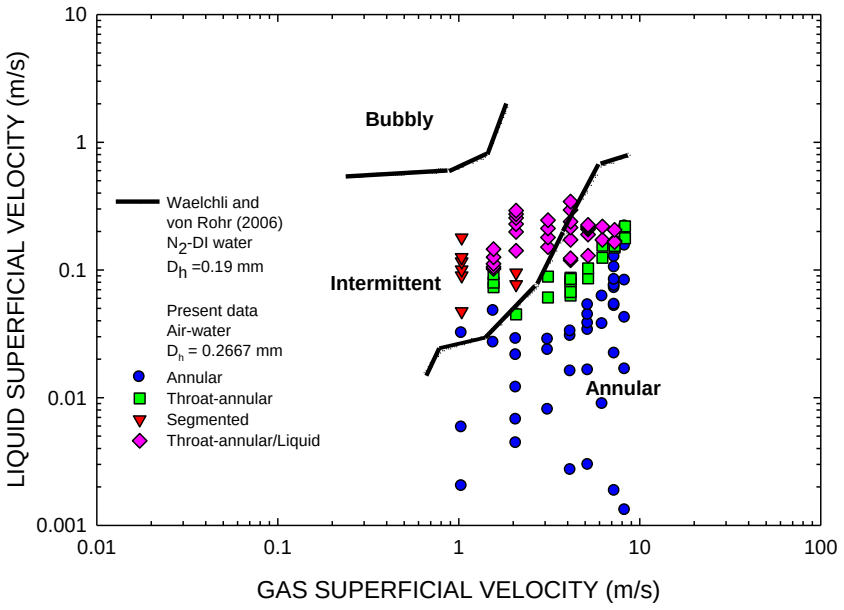

Figure 5.6 Comparison of the observed flow patterns with the transition lines by Waelchli and von Rohr (2006)

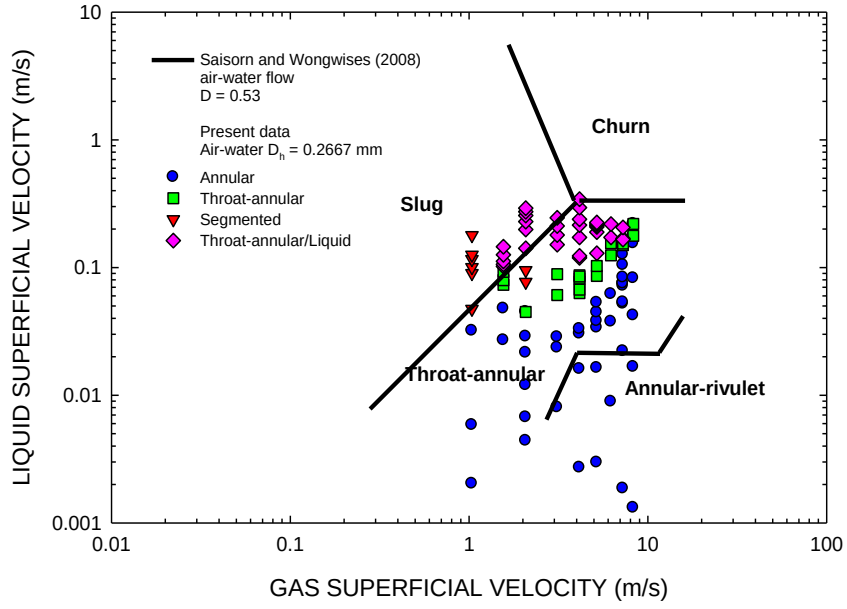

Figure 5.7 Comparison of the observed flow patterns with the transition lines by Saisorn and Wongwises (2008)

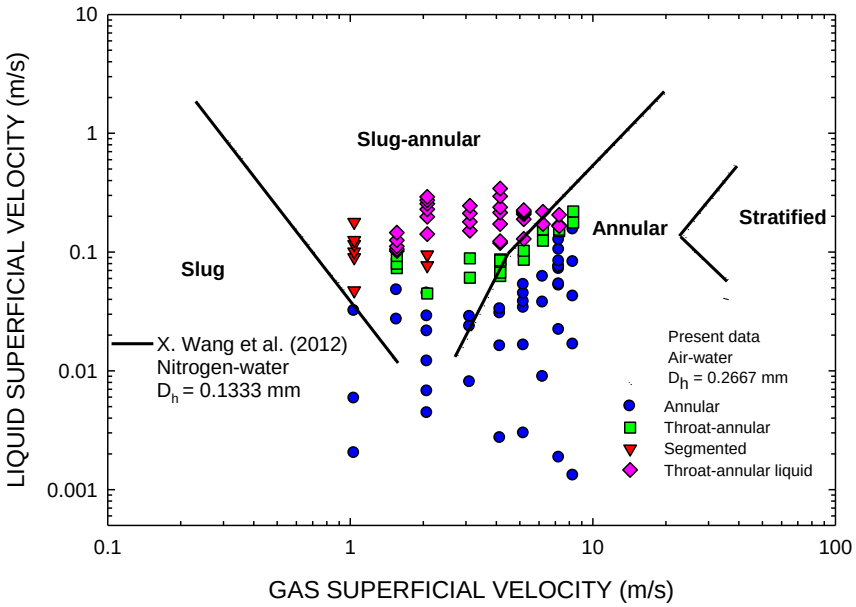

Figure 5.8 Comparison of the observed flow patterns with the transition lines by X. Wang et al. (2012)

The predictions of these authors are in reasonable agreement with the experimental observations in the flow pattern as conclusion of the table 5.1.

Table 5.1 Summary of predictable flow regime maps

Year	Authors	Working fluids	Geometry	Hydraulics diameter (mm)	Well-predicted flow patterns
1999	Triplett et al.	Air-water	Circular	1.097	Segmented, Throat-annular
2002	Kawahara et al.	N_2-DI water	Circular	0.1	Segmented
2004	Qu et al.	Air-water	Rectangular	0.6	Annular
2006	Waelchli and von Rohr	N_2-DI water	Rectangular	0.19	Annular, Segmented
2008	Saisorn and Wongwises	Air-water	Circular	0.53	Annular, Segmented
2012	Wang et al.	N_2-water	Rectangular	0.1333	Throat-annular, Annular

5.2 Pressure drop

5.2.1 Single-phase pressure drop

The single-phase of air and water flow through the channel are the first experiment to investigate the friction factor. In Figures 5.9 and 5.10, the friction factor data calculated from the experiment of single-phase of water both of adiabatic and non-boiling flow are fairly agree well with $f = 62.2/\mathrm{Re}$ that obtained from the conventional sized channel. Nevertheless, the results obtained from air flow are relatively high from $f = 62.2/\mathrm{Re}$ line and rather close to Saisorn and Wongwises's (2008) correlation. For this study, the correlation for laminar air flow is developed and expressed in

$$f = 241.41\mathrm{Re}^{-1.19}$$

.

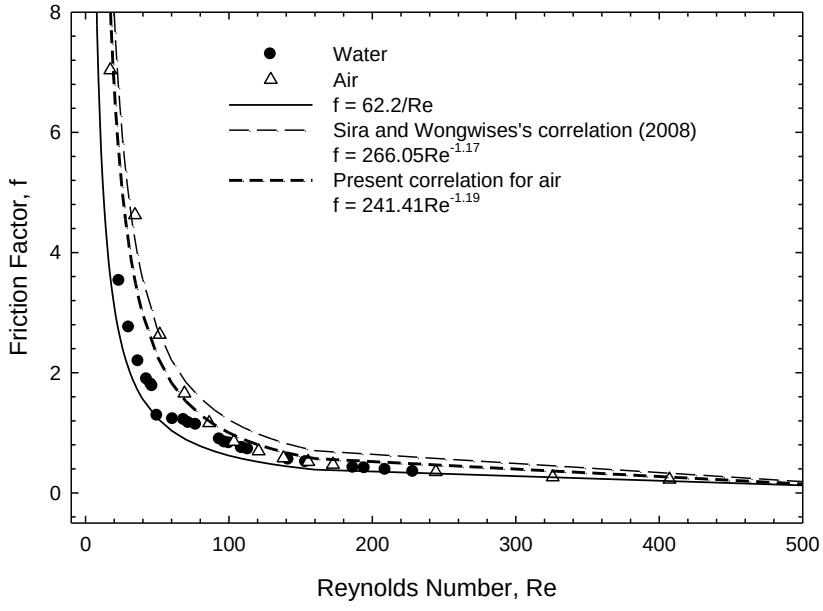

Figure 5.9 Experimental friction factor data for adiabatic air and water flow through a 267 μm mm diameter channel

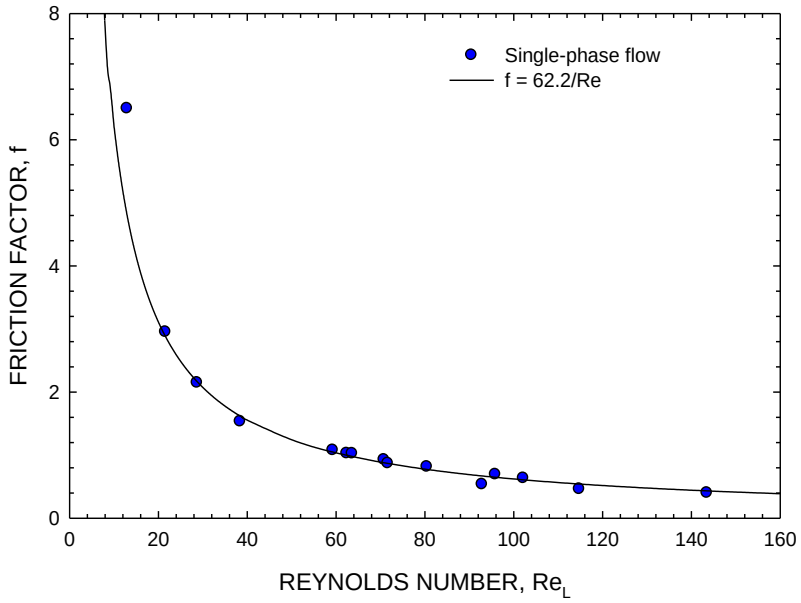

Figure 5.10 Experimental friction factor data for nonboiling water flow through a 267 μm mm diameter channel

5.2.2 Two-phase pressure drop

5.2.2.1 Homogeneous flow model

Figure 5. shows the two-phase friction factor and Reynolds number for various flow patterns by using Awad and Muzychka's two-phase viscosity model, which predicts the two-phase pressure drop of adiabatic segmented, throat-annular, and throat-annular/liquid in the agreement of 30% MAE. However, all existing models over-predicted pressure drop data for annular flow.

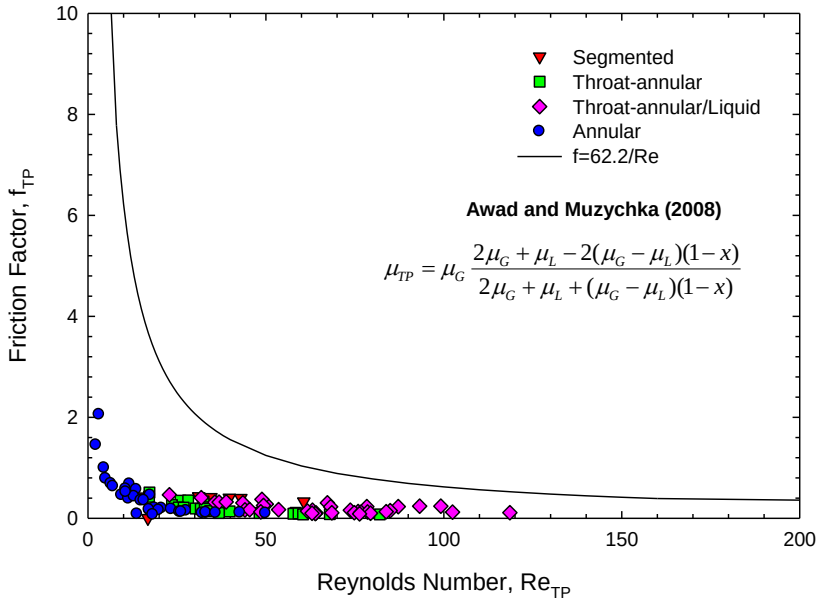

Figure 5.11 Two-phase friction factor and Reynolds number for the various adiabatic flow pattern using Awad and Muzychka's two-phase viscosity model

The predictions with various viscosity models are shown in Table 5.2

Table 5.2 Effective mean viscosity models

Flow pattern	**%MAE of the predictions with various viscosity model**					
	McAdams et al. (1942)	Owen (1961)	Dukler et al. (1964)	Beattie and Whalley (1982)	Lin et al. (1991)	Awad and Muzychka (2008)
Segmented	63.3	35.5	94.2	84.4	44.6	36.1
Throat-annular	61.2	31.1	94.5	88.0	27.7	22.3
Throat-annular/liquid	63.7	31.6	94.7	86.1	42.2	32.4
Annular	65.3	176	91.9	87.6	37.9	83.0

5.2.2.2 Separated flow model

5.2.2.2.1 Adiabatic flow

Figure 5.12 shows a comparison of the two-phase friction multiplier data for various adiabatic flow patterns; the predictions by the Lockhart-Martinelli parameter in comparison with the Friedel correlation are also shown in the same figure as the calculated curve. All the flow pattern data are well correlated with the Friedel

correlation. The results from the calculation agree with the measured data within 30% deviation, irrespective of the working fluid, as shown in Fig. 5.13. Further, we proposed the new correlation to predict the two-phase frictional multiplier which developed based on the experimental data as is offered in

$$\phi_L^2 = \frac{39.403}{X^{0.877}}$$

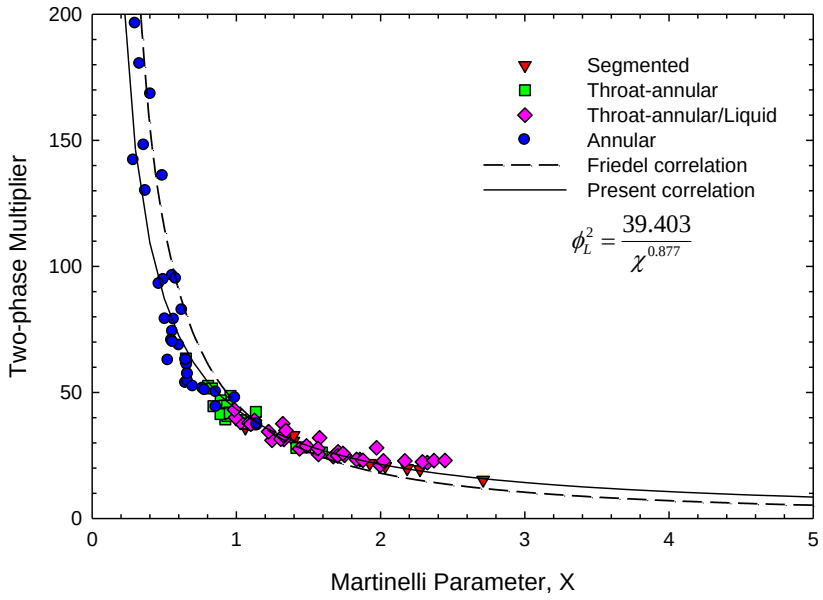

Figure 5.12 Martinelli parameter versus the two-phase frictional multiplier for various adiabatic flow patterns

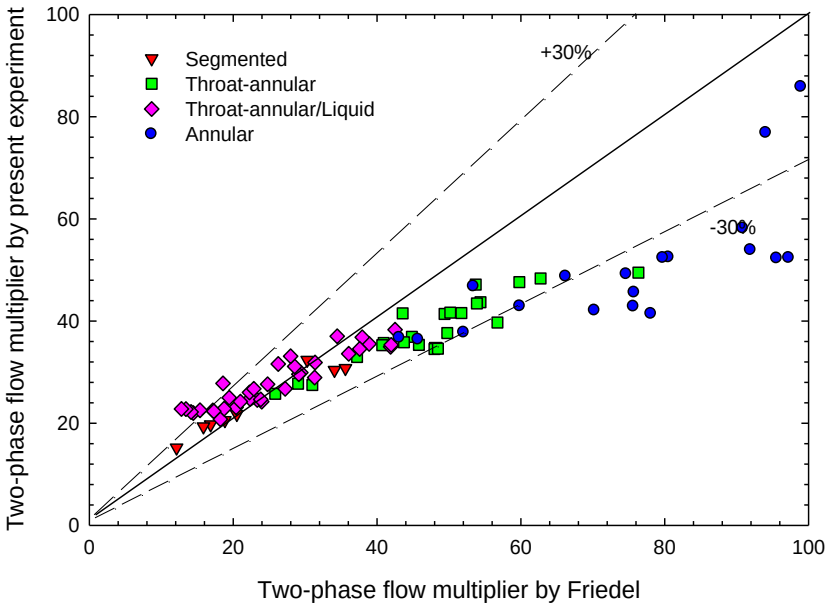

Figure 5.13 Predicted pressure drop by Friedel correlation versus experimental pressure drop for various adiabatic flow patterns

5.2.2.2.2 Nonboiling flow

Figure 5.14 shows the comparison of the Lockhart-Martinelli parameter versus the two-phase frictional multiplier for the nonboiling segmented flow with and without heat transfer and the Friedel correlation.

We found that the two-phase frictional multiplier increased by changing to adiabatic to nonadiabatic flow. Likewise, a comparison between two-phase flow multiplier by Friedel correlation and experimental data is presented in Fig. 5.15, which contains the 35% deviation and provides the predictive accuracy of the corresponding correlations.

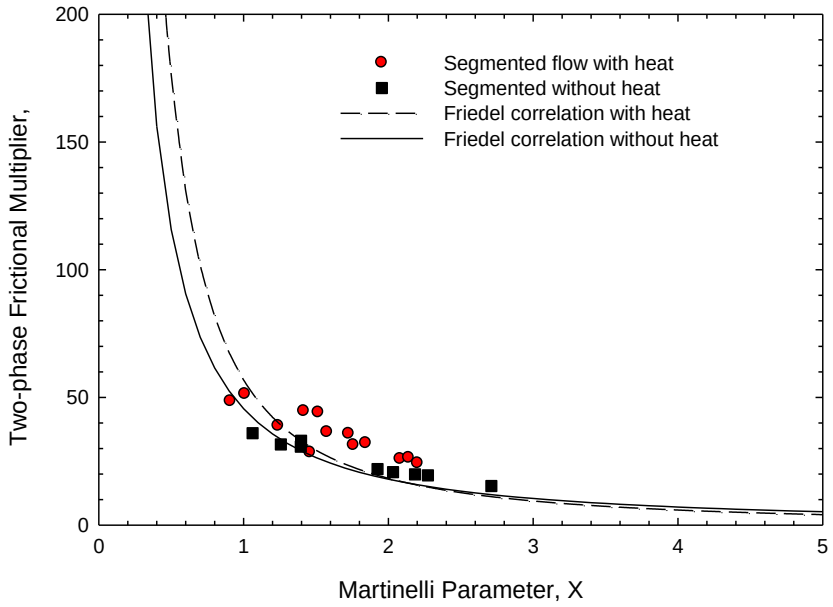

Figure 5.14 Comparison of segmented friction loss with and without heat transfer and the correlation

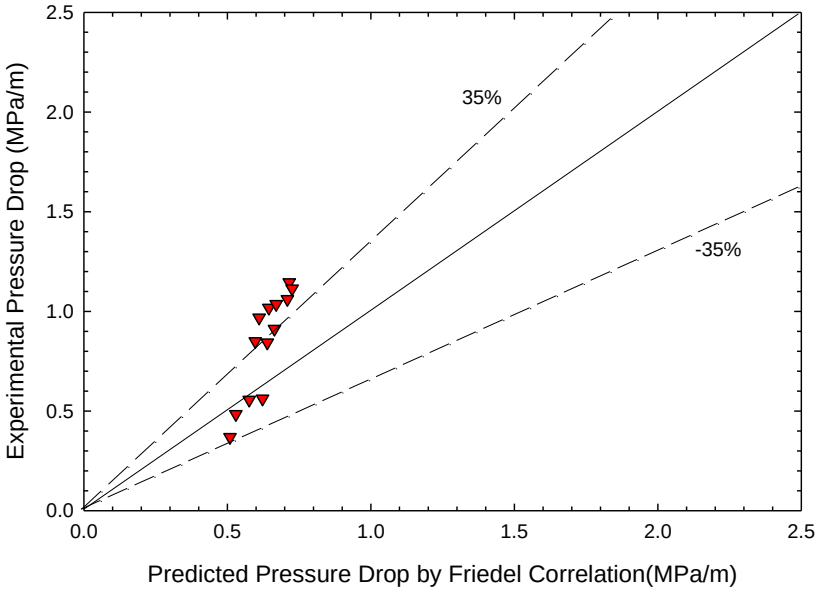

Figure 5.15 Predicted pressure drop by Friedel correlation versus experimental pressure drop for various for nonboiling segmented flow pattern

5.3 Heat transfer characteristics

5.3.1 Single-phase flow

The single-phase and two-phase heat transfer experiment was first conducted to confirm the validity of the experiment setup at as Fig. 5.16 and Fig. 5.17 respectively. The experimental data agree with Wu and Cheng (2003) as Fig. 5.16 and Hetsroni et al. (2009) as Fig. 5.17 which studied heat transfer in the parallel triangular channels of 130 μm in hydraulic diameter.

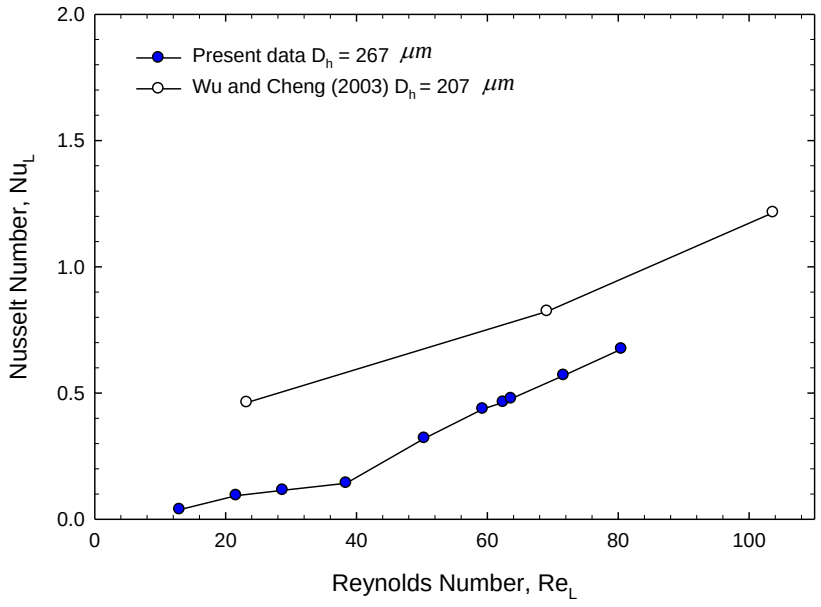

Figure 5.16 The comparison of Nusselt number versus Reynolds with the existing results of other researcher for single-phase flow

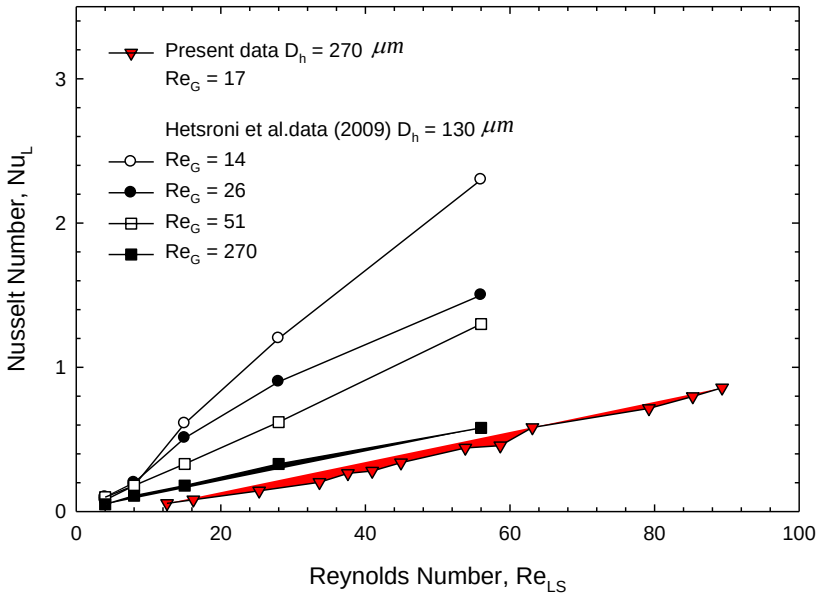

Figure 5.17 The comparison of Nusselt number versus Reynolds with the existing results of other researcher for two-phase flow

5.3.1 Segmented flow

Additionally, Fig. 5.19 shows the segmented flow increases the Nusselt number up to 120% over the single-phase flow in the low Reynolds number range. It should be noted that when the segmented flow changes to another flow pattern, such as what occurs in Fig. 5.18, it is not important to enhance heat transfer with two-phase air-water from single-phase of water anymore. These phenomena are in agreement with the research of Betz and Attinger (2010). Figure 5.20 shows the surface temperature at the channel wall. We found that the wall temperature of single-phase flow is higher than segmented flow. This finding ensures that segmented flow can enhance heat transfer in a rectangular microchannel. The temperature of the surface that increases linearly also indicates that fluid flow through the channel is in the constant heat flux.

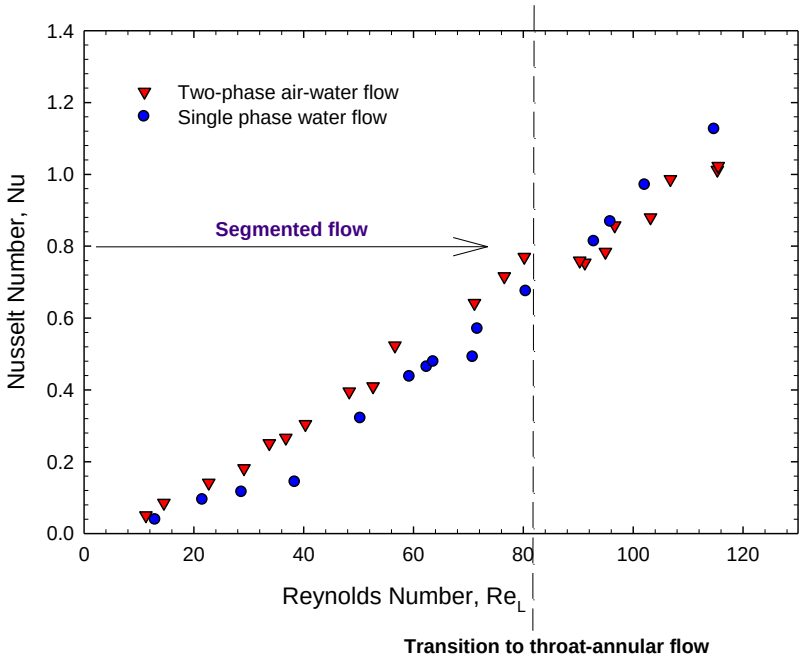

Figure 5.18 Nusselt number of single-phase and two-phase flow versus the Reynolds number with water flow rate at a fixed gas flow rate

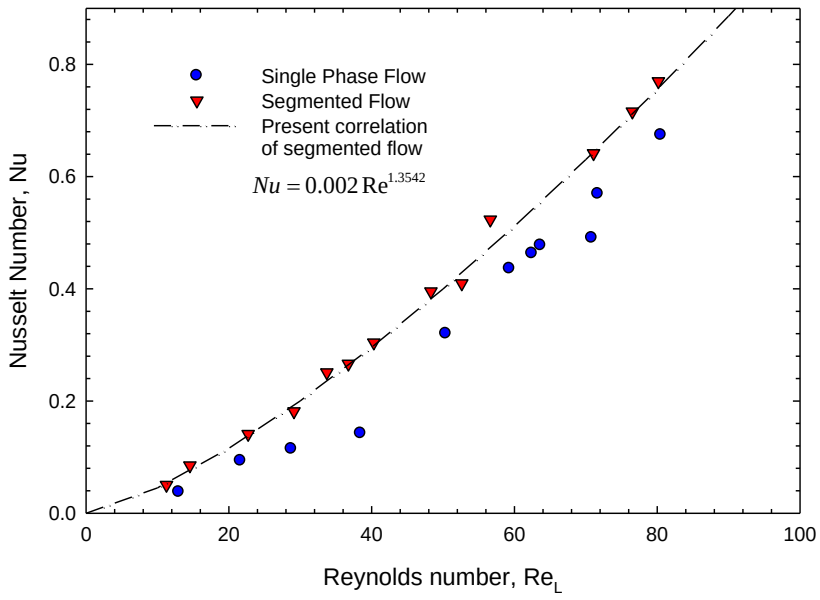

Figure 5.19 The Value of Nusselt number for single-phase and segmented flow versus the Reynolds number with water flow rate at a fixed gas flow rate

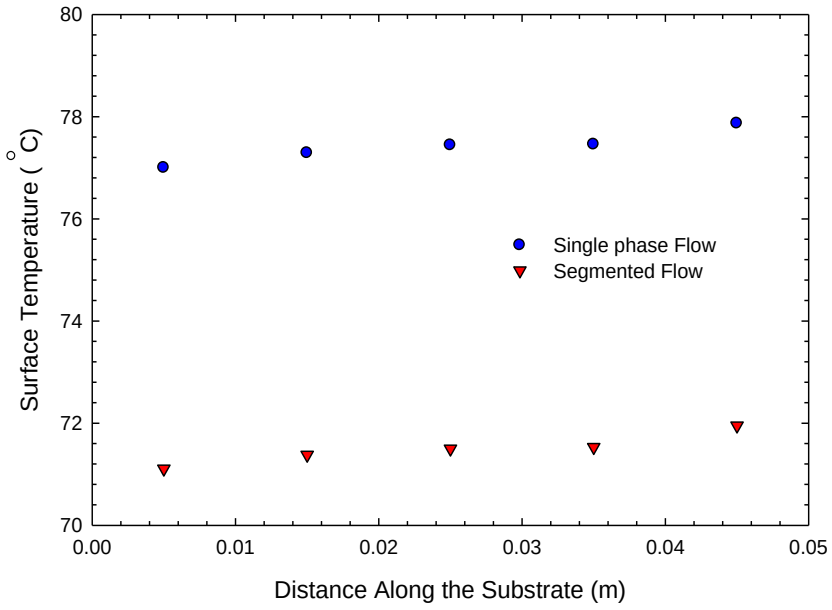

Figure 5.20 Surface temperature, T_s, along the flow direction, for a water flow rate of 7.32×10^{-4} kg/min, in the single phase and segmented flow case

CHAPTER 6 CONCLUSION AND RECOMMENDATIONS FOR FUTURE WORK

This chapter presents the conclusion and recommendations for future work. In the part of conclusion, the important conclusions of this thesis are categorized into subsections as follows:

6.1 Conclusion

The flow pattern images were analyzed to obtain the new transition lines in the flow regime map. The gas superficial velocity and liquid superficial velocity were varied in a range of U_{GS}= 1.038 – 8.302 m/s and U_{LS} = 0.001311- 0.3429 m/s, respectively. The flow patterns including annular flow, segmented flow, throat-annular flow and throat-annular/liquid flow were observed through the stereo-zoom microscope. When comparing the flow regime map to other research, we report a new finding associated with the flow pattern and flow regime map, measured in the lower range of superficial velocity.

The pressure drop in the adiabatic and nonboiling flow was measured and compared with the homogeneous flow model as the various viscosity flow correlations and separated flow model of the Friedel correlation. We found that the Awad and Muzychka (2008) viscosity correlation can predict the frictional pressure drop of segmented, throat-annular and throat-annular/liquid in 30% MAE. The Friedel correlation separated flow model can predict the frictional pressure drop of segmented, throat-annular and throat-annular/liquid of adiabatic flow in 30% deviation and nonboiling segmented flow in 35% deviation.

Segmented air-water flow can enhance heat transfer by up to 120% in a rectangular microchannel, in comparison with single-phase flow at the same liquid flow rate. The Nusselt number was used to characterize the improvement in heat transfer (Betz and Attinger 2010).

6.2 Recommendations for Future Work

The experimental apparatus can be applied for investigating the heat transfer chracteristics of another working fluids and optimize the the test devices, the feature, size, shape and the material of the test-section.

AN EXPERIMENTAL STUDY OF SEGMENTED TWO-PHASE FLOW AND HEAT TRANSFER CHARACTERISTICS IN A MICROCHANNEL

MISS PANSUNEE SUWANKAMNERD

A THESIS SUBMITTED IN PARTIAL FULFILLMENT
OF THE REQUIREMENTS FOR
THE DEGREE OF MASTER OF ENGINEERING
(MECHANICAL ENGINEERING)
FACULTY OF ENGINEERING
KING MONGKUT'S UNIVERSITY OF TECHNOLOGY THONBURI
2013

CURRICULUM VITAE

NAME Ms.Pansunee Suwankamnerd

DATE OF BIRTH 10 January 1986

EDUCATIONAL RECORD

HIGH SCHOOL — High School Education
Benjamarachutit School, 2005

BACHELOR'S DEGREE — Bachelor of Engineering (Mechanical Engineering),
Prince of Songkla University, 2009

MASTER'S DEGREE — Master of Engineering (Mechanical Engineering),
King Mongkut's University of Technology
Thonburi, 2013

SCHOLARSHIP The National Research Council of Thailand (NRCT).

PUBLICATIONS

JOURNAL — Suwankamnerd, P. and Wongwises, S., 2012, Non-boiling of two-phase flow in micro-channels, The Journal of the Royal Institute of Thailand, Vol. 37, pp. 64-80.

REFERENCES

Armand, A.A. and Treschev, G.G., 1946, “The resistance during the movement of a two-phase systems in horizontal pipe”, **Izv Vses Teplotek institute**, Vol. 1, pp. 16-23.

Awad, M.M. and Muzychka, Y.S., 2008, “Effective property models for homogeneous two-phase flows”, **Experimental Themal Fluid Science**, Vol. 33, pp. 106-113.

Betz, A.R. and Attinger, D., 2010, “Can segmented flow enhance heat transfer in microchannel heat sinks?”, **International Journal of Heat and Mass Transfer**, Vol. 53, pp. 3683-3691.

Beattie, D.R.H. and Whalley, P.B., 1982, “A simple two-phase flow frictional pressure drop calculation method”, **International Journal of Multiphase Flow**, Vol. 8, pp. 83-87.

Bretherton, F.P., 1961, “The motion of long bubbles in tubes”, **Journal of Fluid Mechanics**, Vol. 10, pp. 166–188.

Carey, V.P., 1992, **Liquid-vapor phase-change phenomena an introduction to the thermophysics of vaporization and condensation processes in heat transfer equipment**, Taylor and Francis, Hebron, Kentucky, pp. 399-452.

Chisholm, D., 1983, **Two-phase flow in pipeline and Heat Exchangers**, Pitman Press Limited, Bath, England.

Choi, C. and Kim, M., 2011, “Flow pattern based correlations of two-phase pressure drop in rectangular microchannels”, **International Journal of Heat and Fluid Flow**, Vol. 32, pp. 1193-1207.

Choo, K. and Kim, S.J., 2011, “Heat transfer and fluid flow characteristics of nonboiling two-phase flow in microchannels”, **Journal of Heat Transfer**, Vol.133, pp. 102901-1.

Chung, P.M. -Y. and Kawaji, M., 2004, “The effect of channel diameter on adiabatic two-phase flow characteristics in microchannels”, **International Journal of Multiphase Flow**, Vol. 30, pp. 735-761.

Collier, J.G. and Thome, J.R., 1996, **Convective Boiling and Condensation**, Third Edition, Oxford University Press, Oxford, pp. 11-17.

Cubaud, T. and Ho, C.M., 2004, “Transport of bubbles in square microchannels”, **Physics of Fluids**, Vol. 16, pp. 4575-4585.

Damianides, C.A. and Westwater, J.W., 1988, “Two-phase flow patterns in a compact heat exchanger and in small tubes”, **In: Proceedings of the 1st National Conference of the United Kingdom on Heat Transfer**, 14-16 September 1988, Glasgow, Mechanical Engineering Publication, London, pp. 1257-1268.

Dukler, A.E., Wicks, A. and Cleveland, 1964, “Pressure drop and hold-up in two-phase flow: Part A- A comparison of existing correlations and part B-an approach through similarity analysis”. **American Institute of Chemical Engineers Journal**, Vol. 10, pp. 38-51.

Figiola, R.S. and Beasly, D.E., 2006, **Theory and Design for Mechanical Measurements**, fourth edition, Wiley, Hoboken.

Fouilland, T.S. and Fletcher, D.F. and Haynes, B.S., 2010, **Film and slug behaviour in intermittent slug–annular microchannel flows**, Chemical Engineering Science, Vol. 65, pp. 5344–5355.

Friedel, L., 1979, “Improved friction pressure drop correlation for horizontal and vertical two-phase pipe flow”, **European Two-phase Group Meeting**, Ispra, June 1979, Italy, p. E2.

Hetsroni, G., Mosyak, A., Pogrebnyak, E and Segal, Z., 2009, "Heat transfer of gas liquid mixture in micro-channel heat sink", **International Journal of Heat and Mass Transfer**, Vol. 52, pp. 3963-3971.

Janes, N., Muzychka, Y.S., Guy, B., Walsh, E.J. and Walsh, P., 2010, "Heat transfer in gas-liquid and liquid-liquid two phase plug flow systems", **Thermal and Thermomechanical Phenomena in Electronic Systems**, 12th IEEE Intersociety Conference, 2-5 June 2010, Las Vegas, pp. 1-11.

Kawahara, A., Chung, P.M.-Y. and Kawaji, M., 2002, "Investigation of two-phase flow pattern, void fraction and pressure drop in a microchannel", **International Journal of Multiphase Flow**, Vol. 28, pp. 1411-1435.

Kreutzer, M.T., Kapjin, F., Moulijin, J.A. and Heiszwolf, J.J., 2005, "Multiphase monolith reactors: Chemical reaction engineering of segmented flow in microchannels", **Chemical Engineering Science**, Vol. 60, pp. 5895-5916.

Lim, Y.S., Yu, S.C.M. and Nguyen, N.T., 2013, "Flow visualization and heat transfer characteristics of gas-liquid two-phase flow in microtube under constant heat flux at wall", **International Journal of Heat and Mass Transfer**, Vol. 56, pp. 350-359.

Lin, S., Kwok, C.C.K., Li, R.Y., Chen, Z.H., and Chen, Z.Y., 1991, "Local frictional pressure drop during vaporization for R-12 through capillary tubes", **International Journal of Multiphase Flow**, Vol. 17, pp. 95-102.

Lockhart, R.W. and Martinelli, R.C., 1949, "Proposed correlation of data for isothermal two-phase, two component flow in pipes", **Chemical Engineering Progress**, Vol. 45, pp. 39-48.

Majumder, A., Mehta, B. and Khandekar, S., 2013, "Local Nusselt number enhancement during gas-liquid Taylor bubble flow in a square mini-channel: An experimental study", **International Journal of Thermal Sciences**, Vol. 66, pp. 8-18.

McAdams, W.H., Woods and W.K., Bryan, R.L., 1942, "Vaporization inside horizontal tubes in benzene-oil mixture", **ASME Transactions**, Vol.64, p.193.

Owens, W.L., 1961, "Two-phase pressure gradient", **In: International Development in Heat Transfer, Part II**, ASME, New York, pp. 3-368.

Qu, W., Yoon, S.-M. and Mudawar, I., 2004, "Two-phase flow and heat transfer in rectangular microchannels", **Journal of Electronic Packaging**, IEEE, Vol. 126, pp. 288-300.

Saisorn, S and Wongwises, S., 2008, "Flow pattern, void fraction and pressure drop of two-phase flow in a horizontal circular micro-channel", **Experimental Thermal and Fluid Science**, Vol. 32, pp. 748-760.

Satitchaicharoen, P. and Wongwises, S., 2004, "Two-phase flow pattern maps for vertical upward gas-liquid flow in mini-gap channels", **International Journal of Multiphase Flow**, Vol. 30, pp. 225-236.

Serizawa, A., Feng, Z. P. and Kawahara, Z., 2002, "Two-phase flow in microchannels", **Experimental Thermal and Fluid Science**, Vol. 26, pp. 703-714.

Shah, R. K. and London, A. L., 1978, **Laminar flow forced convection in ducts**, Academic Press, New York, pp. 1-477.

Sue, M. and Griffith, P., 1964, "Two-phase flow in capillary tubes", **Journal of Basic Engineering**, Vol. 86, pp. 576-582.

Sur, A. and Liu, D., 2012, "Adiabatic air-water two-phase flow in circular microchannels", **International Journal of Thermal Sciences**, Vol. 53, pp. 18-34.

Talimi, V., Muzychka, Y. S. and Kacabiyik, S., 2012, "A review on numerical studies of slug flow hydrodynamics and heat transfer", **International Journal of Multiphase Flow**, Vol. 39, pp. 88-104.

Thulasidas, T.C., Abraham, M.A. and Cerro, R.L., 1997, “Flow patterns in liquid slugs during bubble-train flow inside capillaries”, **Chemical Engineering Science**, Vol. 52, pp. 2947-2962.

Triplett, K.A., Ghaiaasian, S.M., Adel-Khalik, S.I. and Sadowski, D.L., 1999, “Gas-liquid two-phase flow in microchanels Part I: two-phase flow patterns”, **International Journal of Multiphase Flow**, Vol. 25, pp. 377-394.

Waelchli, S. and von Rohr, P.R., 2006, “Two-phase flow characteristics in gas-liquid microreactors”, **International Journal of Multiphase Flow**, Vol. 32, pp. 791-806.

Wang, X., Yong, Y., Fan, P., Yu, G., Yang, C. and Mao, Z. -S., 2012, “Flow regime transition for cocurrent gas–liquid flow in micro-channels”, **Chemical Engineering Science**, Vol. 69, pp. 578-586.

Wu, H. Y. and Cheng, P., 2003, “An experimental study of convective heat transfer in silicon microchannels with different surface conditions”, **International Journal of Heat and Mass Transfer**, Vol. 46, pp. 2547-2556.

Yue, J., Luo, L., Gonthier, Y., Chen, G. and Yuan, Q., 2009, “An experimental study of air-water Taylor flow and mass transfer inside square microchannels”, **Chemical Engineering Science**, Vol. 64, pp. 3697-3708.

Zhao, T.S. and Bi, Q.C., 2001, “Co-current air-water two-phase flow patterns in vertical triangular micro-channels”, **International Journal of Multiphase Flow**, Vol. 25, pp. 411-432.